Hydrodynamics of isotropic and liquid crystalline active polymer solutions

Aphrodite Ahmadi and M. C. Marchetti
Physics Department, Syracuse University, Syracuse, New York 13244, USA

T. B. Liverpool
Department of Applied Mathematics, University of Leeds, Woodhouse Lane, Leeds LS2 9JT, United Kingdom
(Received 30 June 2006; published 29 December 2006)

We describe the large-scale collective behavior of solutions of polar biofilaments and stationary and mobile crosslinkers. Both mobile and stationary crosslinkers induce filament alignment promoting either polar or nematic order. In addition, mobile crosslinkers, such as clusters of motor proteins, exchange forces and torques among the filaments and render the homogeneous states unstable via filament bundling. We start from a Smoluchowski equation for rigid filaments in solutions, where pairwise crosslink-mediated interactions among the filaments yield translational and rotational currents. The large-scale properties of the system are described in terms of continuum equations for filament and motor densities, polarization, and alignment tensor obtained by coarse-graining the Smoluchovski equation. The possible homogeneous and inhomogeneous states of the systems are obtained as stable solutions of the dynamical equations and are characterized in terms of experimentally accessible parameters. We make contact with work by other authors and show that our model allows for an estimate of the various parameters in the hydrodynamic equations in terms of physical properties of the crosslinkers.

DOI: 10.1103/PhysRevE.74.061913 PACS number(s): 87.16.−b, 47.54.−r, 05.65.+b

I. INTRODUCTION

Soft active systems are a new and exciting class of complex fluids to which energy is continuously being supplied by internal or external sources. Biology provides many examples of such systems, which include cell membranes, biopolymer solutions driven by chemical reactions, collections of living cells moving on a substrate, and the cytoskeleton of eukaryotic cells [1]. The cytoskeleton is a complex three-dimensional network of long filamentary proteins (mainly F-actin and microtubules) cross-linked by a variety of smaller proteins [2,3]. Among the latter are clusters of *active* motor proteins, such as myosin and kinesin, that transform chemical energy from the hydrolysis of ATP (adenosine triphosphate) into mechanical work and are capable of "walking" along the filaments, mediating the exchange of forces between them [4–7].

The self-organization of motor-filament mixtures has been the subject of recent experiments [4–7]. Specifically, mixtures of microtubules and associated motor clusters have been studied in vitro in a confined quasi-two-dimensional geometry [6,7]. Complex patterns, including asters and vortices or spirals have been observed in these in vitro experiments as a function of motor and ATP concentration [6,7]. The high frequency mechanical response of active filament solutions, which are dominated by the bending modes of the filaments, have also been studied both experimentally and theoretically [8–10]. The study of the properties of these simplified model systems paves the way to a better understanding of the formation and stability of more complex structures of biological relevance, such as the mitotic spindle formed during cell division [1].

There have been a number of recent theoretical studies of the collective dynamics of rigid active filaments. First and most microscopic, numerical simulations with detailed modeling of the filament-motor coupling have been used to generate patterns similar to those found in experiments [6,7]. These approaches have given valuable insights into the problem but are limited to small system sizes by computing power. A second very interesting development has been the proposal of "mesoscopic" mean-field kinetic equations governing the dynamics of individual filaments where the effect of motors was incorporated via a motor-induced relative velocity of pairs of filaments, with the form of such velocity inferred from general symmetry considerations [11–15]. Finally, hydrodynamic equations have also been proposed where the large-scale dynamics of the mixture is described in terms of a few coarse-grained fields whose dynamics is also inferred from symmetry considerations [16–25]. Recently, a connection between the mesoscopic and hydrodynamic approaches was established by us by deriving hydrodynamic equations via a coarse-graining of the kinetic equations [26]. This was done in the spirit of polymer physics, which has been successful at predicting macroscopic dynamical behavior of polymer solutions based on models of the microscopic dynamics. To make a link with the motor properties, we consider a simplified model of the motor-filament interaction in Appendix A.

The richness of the phenomena exhibited by the cytoskeleton is illustrated by the ability of its constituents to organize in a variety of different structures. In addition, different constituents can form very similar structures. This leads naturally to the question—how much of the behavior is specific and how much is generic? To answer this question it is important to make the connection between microscopic models and "generic" hydrodynamic approaches.

In this paper we describe a derivation of the hydrodynamic equation for a solution of polar filaments and both stationary and mobile crosslinkers. A brief summary of the approach and some of the results have been presented earlier [26,27]. The filaments are modeled as rigid rods of fixed length. Hydrodynamics is obtained by coarse-graining the

Smoluchowski equation for rods in solution, coupled via excluded volume and motor-mediated interactions. Small protein clusters crosslinking the filaments can be grouped in two classes. The first class comprises stationary crosslinkers, such as α-actinin, that can induce rotation and alignment of the filaments even in the limit of vanishing ATP consumption. Such passive crosslinkers may be polar or nonpolar in nature depending on whether they preferentially bind to pairs of filaments of the same polarity or their binding rate is independent of the filaments' polarity. They always induce filament alignment via a mechanism that has been referred to as the "zipping" effect in the literature [28]. In general, we expect that most crosslinkers will be polar, although "disordered" motor clusters (i.e., cluster with no spatial order in the arrangements of individual motors as in, e.g., *small* myosin clusters) can crosslink filaments regardless of their relative polarity. Stationary crosslinkers can lead to the onset of the homogeneous nematic and polarized states. The interplay between these two types of order is determined by the crosslinkers' polarity. The second class consists of clusters of motor proteins crosslinking two filaments, "active crosslinkers." These can also drive the system into nematic and polarized states. However, in addition by consuming ATP, the motor heads can "walk" along the filaments and mediate the exchange of forces between filaments, inducing filament motion relative to the solution (treated here as an inert background). The motor activity depends crucially on the ATP consumption rate, which is the driving force that sets up and maintains the nonequilibrium state and enters the equation as a chemical potential. Motor activity destabilizes the homogeneous states and induces the formation of spatially inhomogeneous structures on mesoscopic scales, reminiscent of those seen in the in vitro experiments. There are two main motor-mediated mechanisms for force exchange among the filaments. First, active crosslinkers induce bundling of filaments, building up density inhomogeneities. This is the main mechanism responsible for instabilities. It is effective only if the rate at which motor clusters step along the filament is inhomogeneous, which can be due to crowding and fluctuations in the density of bound motors, or to stalling at the polar end. In addition, active crosslinkers sort the filaments according to polarization at a rate proportional to the mean motor stepping rate. This mechanism is important in the polarized state, where it yields filament advection along the direction of polarization and allows for the onset of oscillatory structures.

The forces and torques exchanged by filaments via the crosslinks are described by considering the kinematics of two filaments crosslinked by a single protein cluster that can rotate and translate as a rigid object relative to the filaments. The hydrodynamic equations are then obtained by suitable coarse graining of the Smoluchowski equation. This method yields a general form of hydrodynamics, which incorporates all terms allowed by symmetry, yet it provides a connection between the coarse-grained and the microscopic dynamics. While we have focused here on activity driven by active crosslinks, other active microscopic processes such as treadmilling [1] will lead to hydrodynamics equations of similar form. By comparing the equations obtained here to those obtained from a microscopic model of the forces exchanged between motors and filaments we can relate some of the parameters in the hydrodynamic equations to parameters that can be controlled in experiments.

The hydrodynamic equations are then used to describe the dynamics of the isotropic, nematic, and polarized solutions. We characterize the possible homogeneous states of the system in terms of experimentally accessible parameters and discuss the various mechanisms by which motor activity can destabilize each homogeneous state.

In Sec. II we describe the kinetic model of rods crosslinked by small protein clusters and set up the formalism of the Smoluchowski equation. The dependence of the crosslinked-induced rotational and translational velocities of the filaments on filament orientation and position is obtained from general symmetry considerations and conservation laws. The details of the kinematics of motors and filaments are described in Appendix A, where a specific microscopic model of the coupling is also presented. In Sec. III we obtain the hydrodynamic equations for the system by a systematic coarse graining of the Smoluchowski equation. The full form of the hydrodynamic equations, including diffusive, excluded volume, and active contributions, is given in Appendix C. The nonlinear hydrodynamic equations are solved in Sec. IV to obtain the possible homogeneous steady states of the system. "Phase diagrams" are constructed in terms of the filament and crosslinkers' densities identifying the isotropic, nematic, and polarized states. The nonlinear hydrodynamic equations for each homogeneous state are presented in Sec. V, where the stability of each state is also studied. All homogeneous states become unstable at high filament and crosslinkers' densities via filament bundling. The interplay of bundling and diffusion promotes the onset of stable spatial structures on mesoscopic scales. Finally, we conclude with a discussion of open questions and a comparison with related work.

II. MODEL: SMOLUCHOWSKI EQUATION FOR MOTOR-FILAMENT SOLUTIONS

We model the system as a collection of thin rods of fixed length l and diameter $b \ll l$ crosslinked by small protein clusters (of linear size $\sim b$) that can exchange torques and forces between the filaments. Filaments and crosslinkers move through a solvent, which is assumed inert. The solution forms a quasi-two-dimensional film of thickness much smaller than the length of the filaments. The results presented here should also be relevant to a solution with a distribution of rod lengths, provided such a distribution is sufficiently narrow, i.e., $\sqrt{\langle l^2\rangle - \langle l\rangle^2} \ll \langle l\rangle$. Strong polydispersity in the lengths of rods may lead to more complex behavior. The quasi-two-dimensional geometry gives a good description of a number of physical situations, including the actin lamellipodium of a cell crawling on a substrate and purified filament-motor mixtures studied in vitro. The dynamics of both filaments and crosslinkers is overdamped. This is a good model for a quiescent solution with no externally imposed flow or net flow generated by motor activity. We are interested in describing the filament dynamics on time scales large compared to the characteristic times for binding and

unbinding of the crosslinkers so that we can treat a constant fraction of them as bound. The dynamics of crosslinkers' binding and unbinding was considered for instance in Ref. [25] and it was found that varying the rates of the binding and unbinding of motor clusters did not affect the nature of the nonequilibrium steady states of the active solution. The temperature of the system is taken to be constant and the effect of thermal fluctuations is not considered explicitly. We assume, however, that the stochastic nature of the crosslinkers dynamics, as well as other sources of noise in the systems, can be incorporated in an effective temperature T_a that may differ from the actual temperature of the solution [9,10]. Finally, although the kinetic model described below applies to a solution with a low concentration of filaments, the structure of the continuum equations obtained upon coarse graining the kinetic model is general and not restricted to low density. On the other hand, the quantitative estimates obtained for the various parameters in the hydrodynamic equations are for a low density of filaments and crosslinkers.

The dynamics of the concentration $c(\mathbf{r},\hat{\boldsymbol{u}},t)$ of filaments with center of mass at $\mathbf{r}$ and orientation $\hat{\boldsymbol{u}}$ at time t is governed by the Smoluchowski equation [29,30], which describes the conservation of the number of filaments,

$$\partial_t c = -\boldsymbol{\nabla}\cdot\mathbf{J}_c - \boldsymbol{\mathcal{R}}\cdot\boldsymbol{\mathcal{J}}_c, \tag{2.1}$$

where $\boldsymbol{\mathcal{R}}=\hat{\boldsymbol{u}}\times\partial_{\hat{\boldsymbol{u}}}$ is the rotation operator. The *translational* current density $\mathbf{J}_c$, and *rotational* current density $\boldsymbol{\mathcal{J}}_c$, are given by

$$J_{ci} = -D_{ij}\nabla_j c - \frac{D_{ij}}{k_B T_a} c\nabla_j V_{\mathrm{ex}} + J^A_{ci}, \tag{2.2}$$

$$\mathcal{J}_{ci} = -D_r\mathcal{R}_i c - \frac{D_r}{k_B T_a} c\mathcal{R}_i V_{\mathrm{ex}} + \mathcal{J}^A_{ci}, \tag{2.3}$$

where $D_{ij}=D_{\parallel}\hat{u}_i\hat{u}_j+D_{\perp}(\delta_{ij}-\hat{u}_i\hat{u}_j)$ is the translational diffusion tensor and D_r is the rotational diffusion rate. For a low-density solution of long, thin rods $D_{\perp}=D_{\parallel}/2\equiv D/2$, where $D=k_BT_a\ln(l/b)/(2\pi\eta l)$, with η the solvent viscosity, and $D_r=6D/l^2$. The potential V_{ex} incorporates excluded volume effects, which give rise to the nematic transition in a solution of hard rods. It can be written by generalizing the Onsager interaction to inhomogeneous systems as k_BT_a times the probability of finding another rod within the interaction area of a given rod (see Fig. 1). In two dimensions this gives

$$\begin{aligned} V_{\mathrm{ex}}(\mathbf{r}_1,\hat{\boldsymbol{u}}_1) &= k_BT_a\int d\mathbf{r}_2\int d\hat{\boldsymbol{u}}_2 c(\mathbf{r}_2,\hat{\boldsymbol{u}}_2,t)|\hat{\boldsymbol{u}}_1\times\hat{\boldsymbol{u}}_2| \\ &\times\int_{s_1s_2}\delta(\mathbf{r}_1+\hat{\boldsymbol{u}}_1s_1-\mathbf{r}_2-\hat{\boldsymbol{u}}_2s_2) \\ &= k_BT_a\int d\hat{\boldsymbol{u}}_2\int_{s_1s_2}|\hat{\boldsymbol{u}}_1\times\hat{\boldsymbol{u}}_2|c(\mathbf{r}_1+\boldsymbol{\xi},\hat{\boldsymbol{u}}_2,t), \end{aligned} \tag{2.4}$$

where s_i, with $-l/2\leq s_i\leq l/2$, parametrizes the position along the length of the ith filament, for $i=1,2$, and $\int_{s_i}\cdots\equiv\int_{-l/2}^{l/2}ds_i\cdots$. The δ function ensures that the filaments

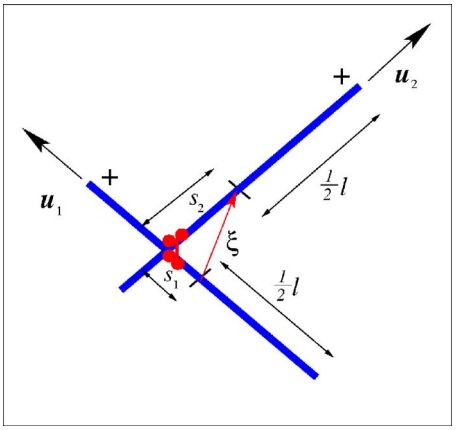

FIG. 1. (Color online) The geometry of overlap between two interacting filaments of length l crosslinked by an active cluster. The crosslink is a distance s_1 (s_2) from the center of mass of filament 1 (2). The distance between centers $\boldsymbol{\xi}=\mathbf{r}_2-\mathbf{r}_1=s_1\hat{\boldsymbol{u}}_1-s_2\hat{\boldsymbol{u}}_2$.

be within each other's interaction volume, i.e., in the thin rod limit $b\ll l$ considered here, have a point of contact. The factor $|\hat{\boldsymbol{u}}_1\times\hat{\boldsymbol{u}}_2|$ represents the excluded area of two thin filaments of orientation $\hat{\boldsymbol{u}}_1$ and $\hat{\boldsymbol{u}}_2$ touching at one point. In the second equality we let $\boldsymbol{\xi}=\mathbf{r}_2-\mathbf{r}_1=\hat{\boldsymbol{u}}_1s_1-\hat{\boldsymbol{u}}_2s_2$ [29].

The translational and rotational active current of filaments with center of mass at $\mathbf{r}_1$ and orientation along $\hat{\boldsymbol{u}}_1$ are written as

$$\begin{aligned} \mathbf{J}^A_c(\mathbf{r}_1,\hat{\boldsymbol{u}}_1) &= b^2\int_{\hat{\boldsymbol{u}}_2}\int_{s_1s_2}|\hat{\boldsymbol{u}}_1\times\hat{\boldsymbol{u}}_2|\, m(\mathbf{r}_1+\hat{\boldsymbol{u}}_1s_1)\mathbf{v}_1(s_1,s_2,\hat{\boldsymbol{u}}_1,\hat{\boldsymbol{u}}_2) \\ &\times c(\mathbf{r}_1,\hat{\boldsymbol{u}}_1,t)c(\mathbf{r}_1+\boldsymbol{\xi},\hat{\boldsymbol{u}}_2,t), \end{aligned} \tag{2.5}$$

$$\begin{aligned} \mathcal{J}^A_c(\mathbf{r}_1,\hat{\boldsymbol{u}}_1) &= b^2\int_{\hat{\boldsymbol{u}}_2}\int_{s_1s_2}|\hat{\boldsymbol{u}}_1\times\hat{\boldsymbol{u}}_2|\, m(\mathbf{r}_1+\hat{\boldsymbol{u}}_1s_1)\boldsymbol{\omega}_1(s_1,s_2,\hat{\boldsymbol{u}}_1,\hat{\boldsymbol{u}}_2) \\ &\times c(\mathbf{r}_1,\hat{\boldsymbol{u}}_1,t)c(\mathbf{r}_1+\boldsymbol{\xi},\hat{\boldsymbol{u}}_2,t), \end{aligned} \tag{2.6}$$

where $m(\mathbf{r})$ is the density of bound crosslinkers, evaluated at the point of attachment to the filaments. Also, $\mathbf{v}_1=\dot{\mathbf{r}}_1$ is the translational velocity that the center of mass of filament 1 acquires due to the crosslinker-mediated interaction with filament 2, when the centers of mass of the two filaments are separated by $\boldsymbol{\xi}$. Similarly, $\boldsymbol{\omega}_1\times\hat{\boldsymbol{u}}_1=\dot{\hat{\boldsymbol{u}}}_1$ is the crosslinker-induced velocity of rotation about the center of mass (see Fig. 1). This crosslinker-generated motion can be, generalized quite straightforwardly to include dynamics generated by treadmilling where equal rates of polymerization and depolymerization of the ends of the filament keep the filament length constant [1] but add a similar contribution to the translational current.

Small clusters of motor proteins crosslinking two filaments can be stationary or mobile (active). In general the density of bound crosslinkers can be written as $m=m_s+m_a$, with m_s and m_a the densities of stationary and mobile crosslinks, respectively. Mobile crosslinks are clusters of motor proteins that can diffuse and be convected along the filaments. The mobile crosslinker density obeys a diffusion-convection equation given by

$$\partial_t m_a = D_m \nabla^2 m_a - \nabla \cdot \mathbf{J}_m, \tag{2.7}$$

where

$$\mathbf{J}_m = \frac{b^2}{l} \int_{\hat{\mathbf{u}}} \int_s \hat{\mathbf{u}}\, u(s) c(\mathbf{r}, \hat{\mathbf{u}}, t)\, m_a(\mathbf{r} + \hat{\mathbf{u}} s, t), \tag{2.8}$$

and $u(s)$ is the speed at which a motor cluster steps on a filament at position s. The mean value $u_0 = \int_s u(s)/l$ of the stepping rate is $u_0 \sim aR_{ATP}$, where a is the step size and R_{ATP} is the ATP consumption rate. For typical motor clusters (kinesins on microtubules or myosins on F-actin) $u_0 \sim$ nm/ms [2]. As shown in Ref. [31], spatial inhomogeneities in the motor stepping rate $u(s)$, especially the stalling of motors at the polar end, are crucial for driving filament bundling and pattern formation. Such inhomogeneities may arise from motor crowding or from large fluctuations in the concentration of ATP under the condition of near depletion. Very recent experiments in purified actin-myosin II solutions have indeed suggested that the motor-driven formation of spatially inhomogeneous patterns, such as asters and vortices, may be associated with strong inhomogeneities in motor activity [32].

The translational and rotational velocities of the filaments induced by crosslinkers are written in a general form that is consistent with translational and rotational invariance. We consider a pair of filaments cross-linked by a single protein cluster. As seen below, all crosslinkers can exchange torque among the filament and induce filament alignment or zipping. Mobile crosslinkers that consume ATP to step along filaments can also exchange forces and induce translational motion of the filaments. In general the rotational and translational dynamics induced by the crosslinkers is coupled.

It is convenient to introduce the relative velocity and net velocity of the filament pair as

$$\mathbf{v} = \mathbf{v}_1 - \mathbf{v}_2,$$

$$\mathbf{V} = \frac{\mathbf{v}_1 + \mathbf{v}_2}{2}, \tag{2.9}$$

with $\mathbf{v}_{1,2} = \mathbf{V} \pm \mathbf{v}/2$. A general form of the relative linear velocity $\mathbf{v}$ and angular velocity $\boldsymbol{\omega} = \boldsymbol{\omega}_1 - \boldsymbol{\omega}_2$ of the filament pair consistent with symmetries and conservation laws is

$$\mathbf{v} = \frac{\tilde{\alpha}(\theta)}{2l} \boldsymbol{\xi} + \frac{\beta(\theta)}{2} (\hat{\mathbf{u}}_2 - \hat{\mathbf{u}}_1), \tag{2.10}$$

$$\boldsymbol{\omega} = 4\gamma(\theta)(\hat{\mathbf{u}}_1 \times \hat{\mathbf{u}}_2), \tag{2.11}$$

where $\boldsymbol{\xi} = \hat{\mathbf{u}}_1 s_1 - \hat{\mathbf{u}}_2 s_2$ is the separation of the filaments' centers of mass, and $\tilde{\alpha}$, β, and γ depend on the relative orientation of the two filaments through the angle $\theta = \cos^{-1}(\hat{\mathbf{u}}_1 \cdot \hat{\mathbf{u}}_2)$. The angular dependence of $\tilde{\alpha}$, β, and γ arises both from the kinematics of the crosslinker-mediated filament interaction, as well as from the dependence of the probability that a protein cluster binds two filaments on the angle between the filaments at contact.

It is instructive to rewrite the relative velocity $\mathbf{v}$ in terms of two orthogonal vectors as

$$\mathbf{v} = \frac{\tilde{\alpha}(\theta)}{4l}(s_1 - s_2)(\hat{\mathbf{u}}_1 + \hat{\mathbf{u}}_2) + \left[\frac{\beta(\theta)}{2} - \frac{\tilde{\alpha}(\theta)}{4l}(s_1 + s_2) \right] (\hat{\mathbf{u}}_2 - \hat{\mathbf{u}}_1). \tag{2.12}$$

The physical meaning of Eq. (2.12) can be understood by considering a specific microscopic model of the motor-filament coupling, such as the one described in Appendix A. In this model the kinematics of two filaments coupled by a motor cluster is described explicitly in terms of the rate $u(s)$ at which the cluster steps along the filament and the torsional stiffness κ of the cluster [33]. A comparison of Eq. (2.12) with Eq. (A11) assuming a linear dependence of $u(s)$ on s as $u(s) \sim u_0 - u's$, with $u' = -du/ds$, shows that in the microscopic model $\tilde{\alpha}$ and β are independent of the angle θ, with $\beta = u_0$ and $\tilde{\alpha} = 2lu'$. In general we can identify β with the mean rate at which a motor cluster steps along a filament, i.e., $\beta \sim (1/l)\int_s u(s)$, while $\tilde{\alpha}$ is controlled by spatial variation in the stepping rate, with $\tilde{\alpha} \sim 2l \max|du/ds|$. It is then apparent that the first term on the right-hand side of Eq. (2.10) arises from the variation in motor activity along the filament, such as the stalling of motors before detaching upon reaching a particular point on the filament. It is proportional to the separation $\boldsymbol{\xi}$ of the filaments' centers of mass and vanishes when these coincide. The angular dependence of $\tilde{\alpha}$ is chosen so that this contribution to the relative velocity is largest when filaments are parallel. The second term in Eq. (2.10), proportional to β, vanishes for aligned filaments and drives the separation or sorting of antialigned pairs.

For small angles, we can write the functions $\tilde{\alpha}$, β, and γ in the form of expansions in powers of $\hat{\mathbf{u}}_1 \cdot \hat{\mathbf{u}}_2$ as

$$\tilde{\alpha}(\theta) \simeq \tilde{\alpha}_0 + \tilde{\alpha}_1(\hat{\mathbf{u}}_1 \cdot \hat{\mathbf{u}}_2), \tag{2.13}$$

$$\beta(\theta) \simeq \beta_0 + \beta_1(\hat{\mathbf{u}}_1 \cdot \hat{\mathbf{u}}_2), \tag{2.14}$$

where all coefficients are defined positive. It can be shown that within the approximation used below, where we only consider the first three moments of the filament concentration, no new terms are obtained in the continuum equations for such moments when terms of higher order in $\hat{\mathbf{u}}_1 \cdot \hat{\mathbf{u}}_2$ are included in Eqs. (2.13) and (2.14). Contributions of higher order in the angle between the filaments only affect the numerical coefficients of the various parameters in the continuum equations.

The rotational parameter γ can be estimated by describing the crosslinker as a torsional spring of constant κ, as shown in Appendix A, where we find that the rotational rate induced by a single crosslinker does not depend on θ. We estimate $\gamma \sim D_r \kappa / k_B T_a$. In this model we assume that the motor cluster always binds on the side of the smaller angle between the filaments, as shown in Fig. 2. We distinguish between polar clusters that bind preferentially to filaments of the same polarity [Fig. 2(a)] and nonpolar clusters that bind to filaments regardless of their relative polarity [Fig. 2(b)]. The probability for two such classes of protein clusters to bind to filaments will in general depend on the angle θ between the filaments, yielding an angular dependence of the effective rate $\gamma(\theta)$. Again, to lowest order in $\hat{\mathbf{u}}_1 \cdot \hat{\mathbf{u}}_2$ we write

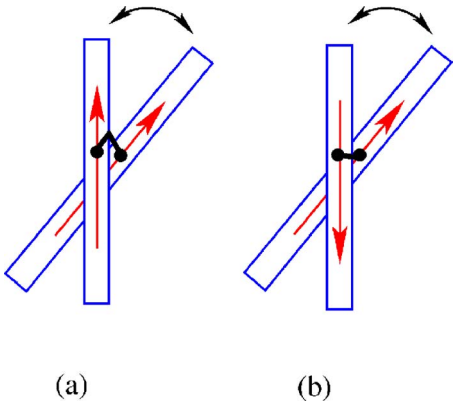

FIG. 2. (Color online) Polar and nonpolar clusters interacting with polar filaments. Assuming that clusters always bind to the smallest angle, polar clusters ($\gamma_P/\gamma_{NP} \gg 1$) bind only to filaments in configuration (a) while nonpolar clusters ($\gamma_P/\gamma_{NP} \ll 1$) bind to both configurations equally.

$$\gamma(\theta) \simeq \gamma_P + \gamma_{NP}(\hat{\boldsymbol{u}}_1 \cdot \hat{\boldsymbol{u}}_2). \tag{2.15}$$

The term proportional to γ_P favors rotations that align filaments of the same polarity and describes polar clusters [6,7], which are in general expected to be active crosslinks in the presence of ATP. The term proportional to γ_{NP} favors rotation in the direction of angles $\theta < \pi$, regardless of the relative polarity of the two filaments. It describes nonpolar clusters, which bind to filament pairs of any orientation [8]. Passive crosslinkers (such as α-actinin on F-actin, which play a crucial role in the rheology of actin gels) [34] can be either polar or nonpolar. Polar clusters ($\gamma_P \neq 0$) were not considered in earlier work by two of us [26], but are crucial for the formation of a polarized phase (see also Ref. [35]). Both γ_P and γ_{NP} will increase with an increasing binding rate of the clusters to the filament. It is interesting to speculate that the kinesin constructs in the experiments by Nedelec *et al.* [6,7] are polar clusters, while the disordered myosin II clusters studied by Humphreys *et al.* [8] may be apolar in nature. We can also imagine that if the binding (unbinding) of the motor clusters does not require ATP, these terms, unlike the active contributions to the translational currents, would be independent of the ATP hydrolysis rate.

To determine the net linear velocity $\mathbf{V}$ and rotational velocity $\boldsymbol{\Omega} = (\omega_1 + \omega_2)/2$ we note that the third law and momentum conservation require that the net force and torque due to a motor cluster on a pair of filaments vanishes in the absence of external forces. This yields

$$\zeta_{ij}(\hat{\boldsymbol{u}}_1) v_{1j} + \zeta_{ij}(\hat{\boldsymbol{u}}_2) v_{2j} = 0, \tag{2.16}$$

$$\zeta_r \boldsymbol{\omega}_1 + \zeta_r \boldsymbol{\omega}_2 = 0, \tag{2.17}$$

where $\zeta_{ij}(\hat{\boldsymbol{u}}) = \zeta_\parallel \hat{u}_i \hat{u}_j + \zeta_\perp(\delta_{ij} - \hat{u}_i \hat{u}_j)$, with $\zeta_\parallel = k_B T_a / D_\parallel$ and $\zeta_\perp = k_B T_a / D_\perp$, is the friction tensor of a long thin rod and $\zeta_r = k_B T_a / D_r$ is the rotational friction. The vanishing of the net torque on the pair clearly requires $\boldsymbol{\omega}_2 = -\boldsymbol{\omega}_1$, i.e., there is no net rotational velocity. The net velocity $\mathbf{V}$ of the pair is generally nonzero and is given by the solution of Eq. (2.16), or

$$[\zeta_{ij}(\hat{\boldsymbol{u}}_1) + \zeta_{ij}(\hat{\boldsymbol{u}}_2)] V_j = -\frac{1}{2}[\zeta_{ij}(\hat{\boldsymbol{u}}_1) - \zeta_{ij}(\hat{\boldsymbol{u}}_2)] v_j. \tag{2.18}$$

Its explicit form is given by

$$\mathbf{V} = A(\hat{\boldsymbol{u}}_1 + \hat{\boldsymbol{u}}_2) + B(\hat{\boldsymbol{u}}_2 - \hat{\boldsymbol{u}}_1), \tag{2.19}$$

with

$$A = -\frac{\sigma}{4} \frac{1 - \hat{\boldsymbol{u}}_1 \cdot \hat{\boldsymbol{u}}_2}{1 - \sigma \hat{\boldsymbol{u}}_1 \cdot \hat{\boldsymbol{u}}_2} \left[\beta(\theta) - \frac{\tilde{\alpha}(\theta)}{2l}(s_1 + s_2) \right], \tag{2.20}$$

$$B = -\frac{\sigma}{4} \frac{1 + \hat{\boldsymbol{u}}_1 \cdot \hat{\boldsymbol{u}}_2}{1 + \sigma \hat{\boldsymbol{u}}_1 \cdot \hat{\boldsymbol{u}}_2} \left[\frac{\tilde{\alpha}(\theta)}{2l}(s_1 - s_2) \right], \tag{2.21}$$

where $\sigma = (\zeta_\perp - \zeta_\parallel)/(\zeta_\perp + \zeta_\parallel) > 0$. For long thin rods $\zeta_\perp = 2\zeta_\parallel$ and $\sigma = 1/3$.

Equations (2.12) and (2.19) display explicitly the even and odd symmetry of $\mathbf{V}$ and $\mathbf{v}$, respectively, under filament exchange. Note that the net velocity $\mathbf{V}$ vanishes for isotropic bodies, i.e., when $\zeta_\parallel = \zeta_\perp$ ($\sigma = 0$).

III. CONTINUUM EQUATIONS

Our goal here is to obtain a set of coarse-grained equations to describe the macroscopic dynamics of active filament mixtures on scales large compared to the filaments' length l and on time scales long compared to the typical binding times of the crosslinkers.

This level of description is valid when the macroscopic quantities describing the solution exhibit spatial variations on length scale much greater than the length of the filaments [30]. The macroscopic quantities we choose to study are the local filament density, $\rho(\mathbf{r},t)$, the local filament polarization, $\mathbf{p}(\mathbf{r},t)$, and the alignment tensor, $S_{ij}(\mathbf{r},t)$, a second-rank symmetric tensor, which measures the local orientational order in a nematic state. These fields are associated with either conservation laws (the density) or possible broken continuous symmetries ($\mathbf{p}, S_{ij}$) and therefore control the hydrodynamic modes of the system. They can be defined as the first three moments of the distribution $c(\mathbf{r},\hat{\boldsymbol{u}},t)$ [26],

$$\rho(\mathbf{r},t) = \int_{\hat{\boldsymbol{u}}} c(\mathbf{r},\hat{\boldsymbol{u}},t),$$

$$\mathbf{T}(\mathbf{r},t) \equiv \rho(\mathbf{r},t)\mathbf{p}(\mathbf{r},t) = \int_{\hat{\boldsymbol{u}}} \hat{\boldsymbol{u}}\, c(\mathbf{r},\hat{\boldsymbol{u}},t),$$

$$Q_{ij}(\mathbf{r},t) \equiv \rho(\mathbf{r},t) S_{ij}(\mathbf{r},t) = \int_{\hat{\boldsymbol{u}}} \hat{Q}_{ij}(\hat{\boldsymbol{u}}) c(\mathbf{r},\hat{\boldsymbol{u}},t), \tag{3.1}$$

with $\hat{Q}_{ij}(\hat{\boldsymbol{u}}) = \hat{u}_i \hat{u}_j - \frac{1}{2}\delta_{ij}$. Hydrodynamic equations for these coarse-grained densities can be obtained by writing an exact moment expansion for $c(\mathbf{r},\hat{\boldsymbol{u}},t)$ (see Appendix B) and truncating this expansion at the third moment. To derive the continuum equations we assume that all quantities are slowly varying on the scales of interest and expand the concentration of filaments $c(\mathbf{r}_1 + \boldsymbol{\xi}, \hat{\boldsymbol{u}}_2)$ and the crosslinker density

$m(\mathbf{r}_1+\hat{\boldsymbol{u}}_1 s_1)$ in the expressions for the active currents near their values at $\mathbf{r}_1$ as

$$c(\mathbf{r}_1+\boldsymbol{\xi},\hat{\boldsymbol{u}}_2)=c(\mathbf{r}_1,\hat{\boldsymbol{u}}_2)+\xi_i\partial_{1i}c(\mathbf{r}_1,\hat{\boldsymbol{u}}_2)+\frac{1}{2}\xi_i\xi_j\partial_{1i}\partial_{1j}c(\mathbf{r}_1,\hat{\boldsymbol{u}}_2)+O(\nabla^3), \quad (3.2)$$

$$m(\mathbf{r}_1+\hat{\boldsymbol{u}}_1 s_1)=m(\mathbf{r}_1)+\hat{u}_{1i}s_1\partial_{1i}m(\mathbf{r}_1)+\frac{1}{2}\hat{u}_{1i}\hat{u}_{1j}s_1^2\partial_{1i}\partial_{1j}m(\mathbf{r}_1)+O(\nabla^3). \quad (3.3)$$

When the expansions (3.2) and (3.3) are inserted in Eqs. (2.5) and (2.6), the integration over s_1 and s_2 can be carried out term by term. An analogous expansion is used to approximately evaluate the excluded volume interaction, as well as in the equation for the motor concentration. Some details of the derivation of the hydrodynamic equations for the motor density, filament density, polarization, and alignment tensor are given in Appendix C.

For simplicity, here we consider the nonlinear continuum equations retaining only terms up to second order in the gradients. While the analysis of the linear stability of homogeneous states with terms up to fourth order in the gradients does introduce a new length scale (see Appendix D), the simplified equations are instructive and capable of describing much of the physics. The motor density obeys a simple diffusion equation given by

$$\partial_t m_a = D_m\nabla^2 m_a - \boldsymbol{\nabla}\cdot(m_a\mathbf{T}), \quad (3.4)$$

where the second term describes convection of the motors along the filaments [18]. The equations for the filament density, polarization, and alignment tensor are

$$\partial_t\rho = -\partial_i J_i, \quad (3.5)$$

$$\partial_t(\rho p_i) = -\partial_j J_{ij} - R_i, \quad (3.6)$$

$$\partial_t(\rho S_{ij}) = -\partial_k J_{ijk} - R_{ij}, \quad (3.7)$$

where the currents are given by

$$J_i(\mathbf{r},t)=\int_{\hat{\boldsymbol{u}}} J_{ci}(\hat{\boldsymbol{u}},\mathbf{r},t), \quad (3.8)$$

$$J_{ij}(\mathbf{r},t)=\int_{\hat{\boldsymbol{u}}} \hat{u}_i J_{cj}(\hat{\boldsymbol{u}},\mathbf{r},t), \quad (3.9)$$

$$J_{ijk}(\mathbf{r},t)=\int_{\hat{\boldsymbol{u}}} \hat{Q}_{ij} J_{ck}(\hat{\boldsymbol{u}},\mathbf{r},t). \quad (3.10)$$

The rotational current does not contribute to the density equation, but it yields the source terms R_i and R_{ij} in the equations for the polarization and alignment tensor. These are given by

$$R_i(\mathbf{r},t)=\int_{\hat{\boldsymbol{u}}} \hat{u}_i\boldsymbol{\mathcal{R}}\cdot\boldsymbol{\mathcal{J}}_c(\hat{\boldsymbol{u}},\mathbf{r},t), \quad (3.11)$$

$$R_{ij}(\mathbf{r},t)=\int_{\hat{\boldsymbol{u}}} \hat{Q}_{ij}\boldsymbol{\mathcal{R}}\cdot\boldsymbol{\mathcal{J}}_c(\hat{\boldsymbol{u}},\mathbf{r},t). \quad (3.12)$$

The explicit form of the translational (3.8)–(3.10) and rotational (3.11) and (3.12) currents is given in Appendix C. The equation for the density ρ has the form of a continuity equation, as required by filament number conservation. The local polarization $\mathbf{p}$ and the alignment tensor S_{ij} define the order parameters needed to characterize the ordered states of the system and are not conserved variables. Each ordered state discussed below will, however, be characterized by a broken orientational symmetry and a corresponding broken symmetry variable (a unit vector along the direction of broken symmetry) whose fluctuations are infinitely long lived at large wavelength, as required for hydrodynamic modes.

IV. HOMOGENEOUS STATES

We begin by identifying the possible homogeneous steady states of the system. The equations for filament density, polarization, and alignment tensor are obtained from Eqs. (3.5)–(3.7) by inserting the expressions for the currents given in Appendix C. In the homogeneous case all contributions to the dynamical equations come from the rotational currents defined in Eqs. (3.11) and (3.12). Their explicit expression is obtained from Appendix C by inserting the expressions for the diffusive [Eqs. (C7) and (C8)], excluded-volume [Eqs. (C12) and (C13)], and active [Eqs. (C23)–(C27)] contributions to the rotational currents in Eqs. (C2) and (C3), and neglecting all gradient terms. In a homogeneous state the motor density must have a constant value, which we write as $\tilde{m}=mb^2$. The equation for the filament concentration, the polarization, and the alignment tensor are then given by

$$\partial_t\rho = 0, \quad (4.1)$$

$$\partial_t p_i = -[D_r-\gamma_P\tilde{m}\rho_0]p_i + [4D_r\rho_0/\rho_N+(\gamma_{NP}-2\gamma_P)\tilde{m}\rho_0]S_{ij}p_j, \quad (4.2)$$

$$\partial_t S_{ij} = -[4D_r(1-\rho_0/\rho_N)-\gamma_{NP}\tilde{m}\rho_0]S_{ij} + 2\gamma_P\tilde{m}\rho_0\left(p_ip_j-\frac{1}{2}\delta_{ij}p^2\right), \quad (4.3)$$

where all filament densities are measured in units of l^2, and $\rho_N=3\pi/2$. In a homogeneous solution the density is constant, $\rho=\rho_0$. The motor-induced rotational rates γ_P and γ_{NP} have dimensions of frequency and represent the effect of polar and nonpolar motor clusters, respectively. For simplicity we denote by $\tilde{m}$ the total dimensionless density of crosslinkers, without distinguishing between stationary and active protein clusters. One can imagine situations, however, where γ_P will in general be proportional to the ATP consumption rate, but the nonpolar coupling γ_{NP} will be only weakly affected by ATP concentration. In the following, all lengths are measured in units of the filament length l and times are measured in units of D_r^{-1}.

There are three possible homogeneous stationary states for the system, obtained by solving Eqs. (4.2) and (4.3) with $\partial_t p_i=0$ and $\partial_t S_{ij}=0$. These are

$$\text{isotropic state } (I): \quad p_i = 0, \quad S_{ij} = 0,$$

$$\text{nematic state } (N): \quad p_i = 0, \quad S_{ij} \neq 0,$$

$$\text{polarized state } (P): \quad p_i \neq 0, \quad S_{ij} \neq 0.$$

At low density the only solution is $p_i=0$ and $S_{ij}=0$ and the system is isotropic (I). The homogeneous isotropic state can become unstable at high filament and/or motor density, as described below.

To discuss the uniform states it is convenient to rewrite Eqs. (4.2) and (4.3) in a more compact form as

$$\partial_t p_i = -a_1 p_i + b_1 \rho_0 S_{ij} p_j, \tag{4.4}$$

$$\partial_t S_{ij} = -a_2 S_{ij} + b_2 \rho_0 \left(p_i p_j - \frac{1}{2} \delta_{ij} p^2 \right). \tag{4.5}$$

The coefficients a_1, b_1, a_2, and b_2 are given by

$$a_1 = 1 - \tilde{m} \gamma_P \rho_0 / D_r, \tag{4.6}$$

$$a_2 = 4[1 - \rho_0/\rho_N - \gamma_{NP} \tilde{m} \rho_0/(4D_r)], \tag{4.7}$$

$$b_1 = 4[\rho_N^{-1} + (\gamma_{NP} - 2\gamma_P)\tilde{m}/(4D_r)], \tag{4.8}$$

$$b_2 = 2\gamma_P \tilde{m}/D_r. \tag{4.9}$$

In the absence of crosslinkers ($\gamma_P=\gamma_{NP}=0$), no homogeneous polarized state with a nonzero mean value of $\mathbf{p}$ is obtained. There is, however, a transition at the density $\rho_N = 3\pi/2$ from an isotropic state with $S_{ij}=0$ to a nematic state with $S_{ij}=S_0\left(n_i n_j - \frac{1}{2}\delta_{ij}\right)$, with $\mathbf{n}$ a unit vector along the direction of broken symmetry. The transition here is identified with the change in sign of the coefficient a_2 of S_{ij} on the right-hand side of Eq. (4.5). A negative value of a_2 that controls the decay rate of S_{ij} signals an instability of the isotropic homogeneous state. This occurs when excluded volume effects dominate at $\rho_0=\rho_N$. The homogeneous state is isotropic for $\rho_0<\rho_N$ and nematic for $\rho_0>\rho_N$. A mean-field description of such a transition, which is continuous in two dimensions (2D) [but first order in three dimensions (3D)], requires that one incorporates cubic terms in S_{ij} in the equation for the alignment tensor. Adding a term $-c_2\rho_0^2 S_{kl}S_{kl}S_{ij}$ to Eq. (4.5) we obtain $S_0=\frac{1}{\rho_0}\sqrt{-2a_2/c_2}=\frac{1}{\rho_0}\sqrt{-8(1-\rho_0/\rho_N)/c_2}$.

If $\gamma_P=0$, but $\gamma_{NP}\neq 0$, there is again no stable polarized state. The presence of a concentration of nonpolar crosslinkers does, however, renormalize the isotropic-nematic (IN) transition, which occurs at a lower filament density given by

$$\rho_{IN}(\tilde{m}) = \frac{\rho_N}{1 + \tilde{m}\gamma_{NP}\rho_N/(4D_r)}. \tag{4.10}$$

The presence on nonpolar crosslinks favors filament alignment and shifts ρ_{IN} downward, as shown in Fig. 3. A qualitatively similar result has been obtained in numerical simulation of a two-dimensional system of rigid filaments interacting with motor proteins grafted to a substrate [36]. In this case the motors promote alignment by exerting longitudinal forces on the filaments. The amount of nematic order

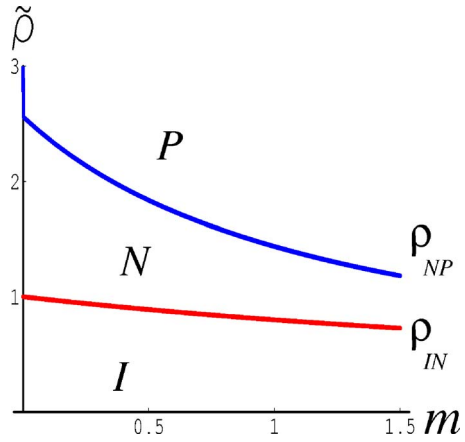

FIG. 3. (Color online) The homogeneous phase diagram for $g<1/4$. For all values of $\tilde{m}$ a region of nematic phase exists between the isotropic and polarized phases ($\gamma_P/D_r=1$, $g=1/10$, and $c_2=50$).

S_0 is also enhanced by motor activity, with $S_0=\frac{1}{\rho_0}\sqrt{-2a_2/c_2}=\frac{1}{\rho_0}\sqrt{-8[1-\rho_0/\rho_{IN}(\tilde{m})]/c_2}$.

If γ_P is finite, the system can order in both polarized and nematic homogeneous states. The homogeneous isotropic state can become unstable in two ways. As in the case $\gamma_P=0$, a change in sign of the coefficient a_2 signals the transition to a nematic (N) state at the density $\rho_{IN}(\tilde{m})$ given in Eq. (4.10). In addition, the isotropic state can become linearly unstable via the growth of polarization fluctuations in any arbitrary direction. This occurs above a second critical filament density,

$$\rho_{IP}(\tilde{m}) = \frac{D_r}{\gamma_P \tilde{m}}, \tag{4.11}$$

defined by the change in sign of the coefficient a_1 controlling the decay of polarization fluctuations in Eq. (4.4). For $\rho_0>\rho_{IP}(\tilde{m})$ the homogeneous state is polarized (P), with $\mathbf{p}\neq 0$. The alignment tensor also has a nonzero mean value in the polarized state as it is slaved to the polarization. The location of the boundaries between the various homogeneous states is controlled by the ratio $g=\gamma_P/\gamma_{NP}$ that measures the polarity of motor clusters. One can identify two scenarios depending on the value of g.

(I) For $g<1/4$, the density ρ_{IP} is always larger than ρ_{IN} and a region of nematic phase exists for all values of $\tilde{m}$. At sufficiently high filament and motor densities, the nematic state becomes unstable. To see this, we linearize Eqs. (4.4) and (4.5) by letting $S_{ij}=S_{ij}^0+\delta S_{ij}$ and $\delta p_i=p_i$. Fluctuations in the alignment tensor are uniformly stable for $a_2<0$, but polarization fluctuations along the direction of broken symmetry become unstable for $a_1 \leqslant \rho_0 b_1 S_0/2$, i.e., above a critical density

$$\rho_{NP} = \frac{D_r}{\tilde{m}\gamma_P}\left[1 + \frac{b_1^2}{c_2 R}\left(1 - \sqrt{1 + \frac{2c_2 R(1-R)}{b_1^2}}\right)\right], \tag{4.12}$$

where $R=\rho_{IN}/\rho_{IP}$. The polarized state at $\rho_0>\rho_{NP}$ has

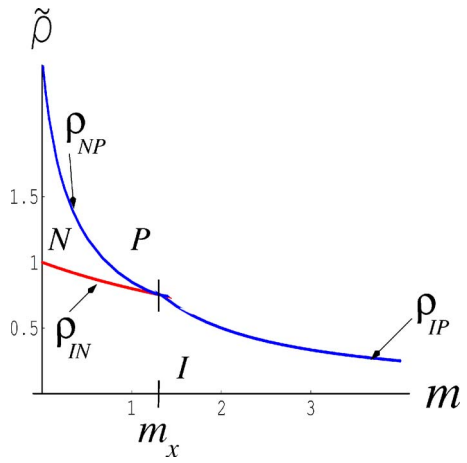

FIG. 4. (Color online) The phase diagram for $g>1/4$. For $\tilde{m}>\tilde{m}_x$, where ρ_{IN} and ρ_{IP} intersect, no N state exists and the system goes directly from the I to the P state ($\gamma_P/D_r=1$, $g=1$, and $c_2=50$).

$$p_i^0 = p_0 \hat{p}_i, \tag{4.13}$$

$$S_{ij}^0 = S_P(\hat{p}_i\hat{p}_j - \delta_{ij}/2), \tag{4.14}$$

with $\hat{\mathbf{p}}$ a unit vector in the direction of broken symmetry and

$$p_0^2 = \frac{2a_1a_2}{\rho_0^2 b_1 b_2}\left[1 - \left(\frac{2a_1}{b_1\rho_0 S_0}\right)^2\right], \tag{4.15}$$

$$S_P = S_0\sqrt{1 - \frac{\rho_0^2 b_1 b_2}{2a_1a_2}p_0^2} = 2\left|\frac{a_1}{\rho_0 b_1}\right|. \tag{4.16}$$

The "phase diagram" for $g<1/4$ is shown in Fig. 3.

(II) When $g>1/4$, the boundaries for the I-N and the N-P transitions cross at

$$\tilde{m}_x = \frac{\rho_N D_r/\gamma_P}{1 - 1/(4g)}, \tag{4.17}$$

where $\rho_{IN}=\rho_{IP}=\rho_{NP}$ and the phase diagram has the topology shown in Fig. 4. For $\tilde{m}>\tilde{m}_x$ the polarity of motor clusters renders the nematic state unstable at all densities larger than $\rho_{IN}(\tilde{m})$ and the system goes directly from the I to the P state at ρ_{IP}, without an intervening N state. At the onset of the polarized state the alignment tensor is again slaved to the polarization field, $S_{ij}=\frac{b_2}{a_2}\rho_0(p_ip_j-\frac{1}{2}\delta_{ij}p^2)$, and $\mathbf{p}=p_0\hat{\mathbf{p}}$. The value of p_0 is determined by cubic terms in Eq. (4.4) not included here.

Finally, we note that if $\gamma_{NP}=0$, with $\gamma_P\neq 0$ (i.e., $g\to\infty$), the I-N transition is independent of motor density and always occurs at $\rho_0=\rho_N$. The motor density where $\rho_{IN}=\rho_{IP}$ reduces to $\tilde{m}_x=\rho_N D_r/\gamma_P$.

Estimates of the various parameters can be obtained using a microscopic model of the motor-filament interaction of the type described in Appendix A. Using parameter values appropriate for kinesin ($\kappa\sim 10^{-22}$ nm/rad [2]) we estimate $\gamma_P\sim\gamma_{NP}\sim\kappa/\zeta_r=\kappa D_r/(k_BT_a)\sim 10^{-1}$ s^{-1}, where we used the value $D_r\sim 10^{-2}$ s^{-1} appropriate for long thin rods in an aqueous solution [37] and $T_a\sim 300$ K. Using $l\sim 10$ μm, $b\sim 10$ nm, the value $\tilde{m}_x$ above which no nematic state exists is found to correspond to a three-dimensional crosslinker density of about 0.5–1 μM for $g=1$ and a sample thickness of order 1 μm. This value is of order of the motor densities used in experiments on purified microtubule-kinesin mixtures such as those of Ref. [8], suggesting that the filament solution in this experiment is always in the polarized state.

V. DYNAMICS OF INHOMOGENEOUS STATES

Experiments on motor-filament mixtures have shown that uniform states are often unstable to the formation of complex spatial structures. These instabilities arise from the growth of spatial fluctuations in the hydrodynamic fields [4–7]. In particular, the rate of motor-induced filament bundling can exceed that of filament diffusion yielding the unstable growth of density inhomogeneities [11–15,26]. States with spatially varying orientational order, where the filaments spontaneously arrange in vortex and aster structures, are also possible [18,25,35]. To understand the different nature of the instability from each homogeneous state, we now examine the dynamics of spatially varying fluctuations in the hydrodynamic fields in each of the stationary homogeneous states of the system. The hydrodynamic fields are those with characteristic decay times that exceed any microscopic relaxation time and become infinitely long at long wavelengths. In other words, in an infinite system (ignoring the boundaries) the spatial Fourier transforms of the fluctuations of the hydrodynamic fields from their steady-state values, $A(\mathbf{k},t)=A(\mathbf{k},0)\exp[-z(\mathbf{k})t]$, decay with a relaxation rate $\mathrm{Re}[z(\mathbf{k})]$ that goes to zero when $\mathbf{k}\to 0$. We find that the low-frequency hydrodynamic modes of this active system are determined by fluctuations in the conserved densities and in variables associated with broken symmetries. A change in sign in the decay rate of these modes signals an instability of the macroscopic state of interest. For simplicity we only discuss here the case of constant motor density. In addition, in this section we let $\alpha_0=\tilde{\alpha}_0/48$, $\alpha_1=\tilde{\alpha}_1/48$ and assume $\alpha_0=\alpha_1=\alpha$, $\beta_0=\beta_1=\beta$. This approximation is justified by the estimate for these motor-induced parameters obtained in Appendix A using a microscopic model for the the motor-mediated filament interaction [31]. We consider separately the spatially varying hydrodynamic modes in each of the homogeneous states: isotropic, nematic, and polarized phases.

A. Isotropic state

The isotropic homogeneous state has $\rho=\rho_0$, $\mathbf{p}_0=0$, and $S_{ij}^0=0$. The only hydrodynamic variable in this state is the density of filaments. The polarization vector $\mathbf{p}$ and nematic orientation tensor S_{ij} are *not* hydrodynamic modes and therefore relax to zero on microscopic time scales. However, due to dynamical constraints such as entanglements, the relaxation of $\mathbf{p}$ and S_{ij} can become sufficiently slow to yield finite lifetime and finite wavelength inhomogeneities [26,38].

The nonlinear equation for the density is given by

$$\partial_t\rho = \frac{3D}{4}\nabla\cdot(1+v_0\rho)\nabla\rho - \alpha\nabla\cdot(\rho\nabla\rho), \tag{5.1}$$

where $v_0=2/\pi$. The active current proportional to α has an effect opposite to that of thermal diffusion as it tends to build

up density inhomogeneities. As we will see below, this term drives filament bundling and is the main pattern-forming mechanism in each of the homogeneous states.

Linear stability

To examine the stability of the isotropic state we consider the dynamics of fluctuations $\delta\rho(\mathbf{r})=\rho(\mathbf{r})-\rho_0$ of the density about its steady-state value ρ_0 to *linear* order in $\delta\rho$. By expanding the fluctuations in Fourier space,

$$\delta\rho(\mathbf{r}) = \Sigma_{\mathbf{k}}\rho_{\mathbf{k}}e^{i\mathbf{k}\cdot\mathbf{r}}, \tag{5.2}$$

the linearized equation for the Fourier amplitudes is given by

$$\partial_t\rho_{\mathbf{k}} = -k^2\left[\frac{3}{4}D(1+\rho_0 v_0) - \alpha\tilde{m}\rho_0\right]\rho_{\mathbf{k}}. \tag{5.3}$$

The relaxation of density fluctuations is governed by a diffusive mode of frequency

$$z_\rho(k) = -k^2\left[\frac{3}{4}D(1+\rho_0 v_0) - \alpha\tilde{m}\rho_0\right]. \tag{5.4}$$

The isotropic state becomes unstable against the growth of density fluctuations if $z_\rho(k)>0$ or $\alpha>\alpha_c$, with

$$\alpha_c = \frac{3D(1+\rho_0 v_0)}{4\tilde{m}\rho_0}. \tag{5.5}$$

Conversely, the homogeneous isotropic state becomes unstable for filament densities larger than a critical value

$$\rho_B^I = \frac{3D}{4\tilde{m}\alpha - 3Dv_0} \sim \frac{3D}{4\tilde{m}\alpha}. \tag{5.6}$$

This bundling instability of the isotropic state has been discussed elsewhere [26,31]. A proper description of the bundling instability requires that one incorporates terms up to fourth order in the gradient expansion of the hydrodynamic fields [38]. The fourth-order terms introduce a new length scale above which the homogeneous state becomes again stable, as shown in Appendix D. The onset of the instability is, however, controlled entirely by the quadratic terms considered here.

B. Nematic state

The homogeneous nematic state is characterized by $\rho=\rho_0$, $\mathbf{p}_0=0$, and $S_{ij}=S_0\left(n_i n_j-\frac{1}{2}\delta_{ij}\right)$, where $\mathbf{n}$ is a unit vector in the direction of broken symmetry, known as the director field. For concreteness we choose $\mathbf{n}=\hat{\mathbf{y}}$. The hydrodynamic fields of such an overdamped nematic liquid crystal are the density and the director. The symmetry of the nematic state requires that the hydrodynamic equations incorporate the symmetry $\mathbf{n}\to-\mathbf{n}$. The magnitude S_0 of the alignment tensor is not a hydrodynamic field and therefore relaxes *quickly* on microscopic time scales to its steady-state value and therefore will be assumed constant below. For simplicity we also neglect excluded volume corrections. The nonlinear hydrodynamic equations for filament density and director field are then given by

$$\begin{aligned}\partial_t\rho = {}& \frac{3D}{4}\left(1-\frac{S_0}{3}\right)\nabla^2\rho - \frac{1}{2}(1-S_0)\alpha\tilde{m}\nabla^2\rho^2 \\ & + \frac{S_0}{2}\partial_i[(D-4\alpha\tilde{m}\rho)n_i n_j\partial_j\rho] \\ & + \frac{S_0}{2}\partial_i\left[\left(D-\frac{4}{3}\alpha\tilde{m}\rho\right)\rho\partial_j(n_i n_j)\right],\end{aligned} \tag{5.7}$$

$$\begin{aligned}\partial_t n_i = {}& \frac{1}{6}\delta_{ij}^T\Bigg\{\left[\frac{7D}{2\rho}+\frac{1}{8}\left(1-\frac{S_0}{2}\right)\gamma_{NP}\tilde{m}\right]\nabla^2(\rho n_j) + \left[\frac{D}{\rho}+\frac{1}{8}(1-S_0)\gamma_{NP}\tilde{m}\right]\partial_j\boldsymbol{\nabla}\cdot(\rho\mathbf{n}) + \left[\frac{D}{\rho}+\frac{1}{8}(1+2S_0)\gamma_{NP}\tilde{m}\right]n_k n_l\partial_l\partial_k(\rho n_j) \\ & - \left[\frac{D}{\rho}\left(1-\frac{3}{4S_0}\right)+\frac{1}{8}\left(1-\frac{1}{2S_0}-\frac{S_0}{2}\right)\gamma_{NP}\tilde{m}\right]n_k\partial_k\partial_j\rho + \left[\frac{D}{\rho}+\frac{1}{8}\left(1+\frac{S_0}{3}\right)\gamma_{NP}\tilde{m}\right]\rho\partial_k(n_k n_l)\partial_l n_j \\ & - \left[\frac{D}{\rho}+\frac{1}{8}\left(1-\frac{S_0}{3}\right)\gamma_{NP}\tilde{m}\right]\rho n_k(\partial_k n_l)\partial_j n_l\Bigg\} - \frac{1}{9}\delta_{ij}^T\alpha\tilde{m}\Bigg\{\frac{3}{2S_0\rho}n_k\partial_k\partial_j\rho^2 + 5S_0\rho\partial_k(n_k n_l)\partial_l n_j + 2S_0\rho n_l(\partial_l n_j)\partial_k n_k \\ & + \left[(5-3S_0)\partial_k n_j + \frac{7}{4}\partial_j n_k + \frac{9}{4}\delta_{jk}\partial_l n_l + 2(2+3S_0)n_k n_l\partial_l n_j\right]\partial_k\rho\Bigg\},\end{aligned} \tag{5.8}$$

where $\delta_{ij}^T=\delta_{ij}-n_i n_j$ projects in the direction transverse to $\mathbf{n}$.

In the density equation [Eq. (5.7)], activity plays the same role as in the isotropic state, with bundling ($\sim\alpha$) opposing diffusion and eventually driving the instability of the homogeneous state, as described below. The first and second terms on the right-hand side of Eq. (5.8) for the nematic director are the elastic restoring forces associated with bend and splay deformations, respectively. These elastic constants are softened by filament bundling, while motor-induced alignment ($\sim\gamma_{NP}$) tends to stabilize the homogeneous nematic state. A solution with $\rho=$constant requires vanishing of splay, i.e., $\boldsymbol{\nabla}\cdot\mathbf{n}=0$. In this limit the director equation reduces to

$$\partial_t n_i = \frac{1}{6}\delta_{ij}^T\Bigg\{\left[\frac{7D}{2}+\frac{1}{8}\left(1-\frac{S_0}{2}\right)\gamma_{NP}\tilde{m}\rho\right]\nabla^2 n_j + \left[D+\frac{1}{8}(1+2S_0)\gamma_{NP}\tilde{m}\rho\right]n_k n_l \partial_l\partial_k n_j + \frac{S_0}{24}\gamma_{NP}\tilde{m}\rho n_k(\partial_k n_l)[\partial_j n_l+\partial_l n_j] - \frac{10S_0}{3}\alpha\tilde{m}\rho n_k(\partial_k n_l)(\partial_l n_j)\Bigg\}. \quad (5.9)$$

In this case bundling does not play any role to linear order.

To discuss the stability of the homogeneous nematic state, we consider the dynamics of spatially varying fluctuations of the hydrodynamic fields about their mean values, by letting

$$\rho(\mathbf{r}) = \rho_0 + \delta\rho(\mathbf{r}), \quad (5.10)$$

$$\mathbf{n}(\mathbf{r}) = \hat{\mathbf{y}} + \delta\mathbf{n}_\perp(\mathbf{r}). \quad (5.11)$$

To lowest order in the fluctuations $\delta\mathbf{n}_\perp$ is perpendicular to $\hat{\mathbf{y}}$, i.e., in the two-dimensional geometry considered here, $\delta\mathbf{n}_\perp = \delta n_x\hat{\mathbf{x}}$. The linearized equation for the Fourier amplitude of density and director fluctuations for $S_0=1$ are given by

$$\partial_t\rho_{\mathbf{k}} = -\frac{1}{2}[Dk^2+(D-4\alpha\tilde{m}\rho_0)k_y^2]\rho_{\mathbf{k}} - \left(D-\frac{4}{3}\alpha\tilde{m}\rho_0\right)\rho_0 k_x k_y n_{\mathbf{k}}, \quad (5.12)$$

$$\partial_t n_{\mathbf{k}} = -\frac{1}{4}\left[\left(3D+\frac{1}{24}\gamma_{NP}\tilde{m}\rho_0\right)k^2+\frac{1}{4}\gamma_{NP}\tilde{m}\rho_0 k_y^2\right]n_{\mathbf{k}} - \frac{1}{8}\left(D-\frac{8}{3}\alpha\tilde{m}\rho_0\right)k_x k_y\frac{\rho_{\mathbf{k}}}{\rho_0}. \quad (5.13)$$

The hydrodynamic modes in the nematic state describe the coupled decay of density and director fluctuations. They are always diffusive and are given by

$$z_\pm(k,\phi) = -\mathcal{D}_\pm^N(\phi)k^2, \quad (5.14)$$

where

$$\mathcal{D}_\pm^N(\phi) = \frac{1}{4}\Bigg\{\frac{5}{2}D+\frac{1}{48}\gamma_{NP}\tilde{m}\rho_0+\left(D+\frac{1}{8}\gamma_{NP}\tilde{m}\rho_0 - 4\alpha\tilde{m}\rho_0\right)\cos^2\phi\Bigg\} \mp \frac{1}{4}\Bigg\{\left[\frac{1}{2}D+\frac{1}{48}\gamma_{NP}\tilde{m}\rho_0 - \left(D-\frac{1}{8}\gamma_{NP}\tilde{m}\rho_0-4\alpha\tilde{m}\rho_0\right)\cos^2\phi\right]^2 + 2\left(D-\frac{4}{3}\alpha\tilde{m}\rho_0\right)\left(D-\frac{8}{3}\alpha\tilde{m}\rho_0\right)sin^2\phi\cos^2\phi\Bigg\}^{1/2}, \quad (5.15)$$

and ϕ is the angle between the wave vector $\mathbf{k}$ and the direction of the broken symmetry $\hat{\mathbf{y}}$. To gain some insight in the angular dependence of the modes it is useful to consider the behavior for special directions of the wave vector. For wave vectors $\mathbf{k}$ along the $\hat{\mathbf{y}}$ direction ($\phi=0$), density and director fluctuations decouple and we obtain

$$z_\rho(k_y) = -[D-2\alpha\tilde{m}\rho_0]k_y^2, \quad (5.16)$$

$$z_n(k_y) = -\frac{1}{4}\left[3D+\frac{7}{24}\gamma_{NP}\tilde{m}\rho_0\right]k_y^2. \quad (5.17)$$

In this case the director fluctuations are always stable, while the density fluctuations become unstable for filament densities above a critical value ρ_B^N given by

$$\rho_B^N(\phi=0) = \frac{D}{2\tilde{m}\alpha}. \quad (5.18)$$

For $\mathbf{k}$ along $\hat{\mathbf{x}}$ ($\phi=\pi/2$) density and director fluctuations again decouple, but both eigenvalues are always negative, with

$$z_\rho(k_x) = -\frac{1}{2}Dk_x^2, \quad (5.19)$$

$$z_n(k_x) = -\frac{1}{4}\left[3D+\frac{1}{24}\gamma_{NP}\tilde{m}\rho_0\right]k_x^2. \quad (5.20)$$

The homogeneous nematic state is linearly stable for all parameter values against long-wavelength fluctuations that only exhibit spatial variation in the direction normal to that of the mean filament orientation.

In general, the critical filament density $\rho_B^N(\phi)$, above which the homogeneous nematic state is unstable, has a complicated angular dependence. It increases with ϕ and it diverges for $\phi\to\pi/2$, where the homogeneous state is linearly stable for all filament density. This angular dependence is shown in Fig. 5 for a few values of parameters.

For all angles the instability is controlled by the bundling rate α, while the rotational rate γ_{NP} always tends to stabilize the homogeneous nematic state.

C. Polarized state

The homogeneous polarized state is characterized by $\rho=\rho_0$, $\mathbf{p}_0=p_0\hat{\mathbf{p}}$, and $S_{ij}^0=S_P\left(\hat{p}_i\hat{p}_j-\frac{1}{2}\delta_{ij}\right)$, with $\hat{\mathbf{p}}$ a unit vector pointing along the direction of broken symmetry. The hydrodynamic fields are the filament density and the unit vector $\hat{\mathbf{p}}$. The magnitude p_0 of the polarization is not a hydrodynamic field and therefore relaxes *quickly* on microscopic time scales to its steady-state value and will be assumed constant in the following. In the polarized state the alignment tensor is slaved to the polarization and does not yield any additional hydrodynamic field. Assuming for simplicity $p_0=1$ and neglecting excluded volume corrections, the nonlinear hydrodynamic equations for filament density and polarization direction are given by [39]

$$\partial_t\rho - \frac{7}{36}\beta\tilde{m}\,\boldsymbol{\nabla}\cdot(\rho^2\hat{\mathbf{p}}) = \frac{3}{4}D\nabla^2\rho - \frac{3}{4}\alpha\tilde{m}\nabla^2\rho^2 - \frac{1}{2}\alpha\tilde{m}\partial_i\partial_j(\rho^2\hat{p}_i\hat{p}_j) \quad (5.21)$$

and

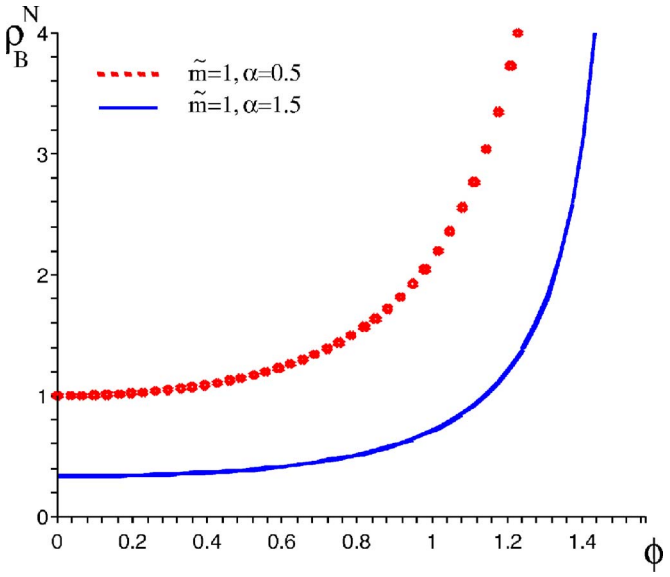

FIG. 5. (Color online) The critical filament density $\rho_B^N(\phi)$ where the homogeneous nematic state becomes linearly unstable is shown as a function of the angle ϕ between the wave vector $\mathbf{k}$ and the direction of broken symmetry for $D=1$, $\gamma_{NP}=1$, $\tilde{m}=1$ and two values of α. At $\phi=0$ the critical density is given by Eq. (5.18). When either α or $\tilde{m}$ are increased, the density $\rho_B^N(\phi)$ shifts to lower values at all angles and the region of stability of the homogeneous nematic state shrinks.

$$\left[\partial_t + \frac{\tilde{m}}{36}\beta\rho\hat{\mathbf{p}}\cdot\boldsymbol{\nabla}\right]\hat{p}_i = \frac{13\tilde{m}}{36}\beta\delta_{ij}^T\partial_j\rho + \frac{1}{96}\gamma_{NP}\tilde{m}\delta_{ij}^T\hat{p}_k\partial_k\partial_j\rho + \delta_{ij}^T\left[\left(\frac{5D}{8\rho}+\frac{\gamma_P\tilde{m}}{24}\right)\nabla^2(\rho\hat{p}_j) + \frac{D}{4\rho}\partial_j\boldsymbol{\nabla}\cdot(\rho\hat{\mathbf{p}})\right] - \frac{\alpha\tilde{m}}{4\rho}\delta_{ij}^T\partial_k\{\rho[\partial_j(\rho\hat{p}_k)+\partial_k(\rho\hat{p}_j)+\delta_{jk}\boldsymbol{\nabla}\cdot(\rho\hat{\mathbf{p}})]\} - \frac{\alpha\tilde{m}}{3\rho}\delta_{ij}^T[2\partial_k(\rho\hat{p}_k\partial_j\rho)+\partial_k(\rho\hat{p}_j\partial_k\rho)+\partial_j(\rho\hat{\mathbf{p}}\cdot\boldsymbol{\nabla}\rho)], \tag{5.22}$$

where

$$\delta_{ij}^T(\hat{\mathbf{p}}) = \delta_{ij} - \hat{p}_i\hat{p}_j, \tag{5.23}$$

projects in the direction transverse to $\hat{\mathbf{p}}$. The usual elastic constants K_1 and K_3 for splay and bend deformations, respectively, can be identified as $K_3 \sim 5D/8$ and $K_1 - K_3 \sim D/4$.

The first term on the right-hand side of the density equation [Eq. (5.21)] is simply filament diffusion. The second term proportional to α opposes diffusion and describes the effect of filament bundling. Finally, the last term describes higher-order nonequilibrium couplings between density and polarization.

The broken directional symmetry of the polarized state yields an effective drift velocity $\sim\beta\tilde{m}\rho\hat{\mathbf{p}}$ describing filament advection along the direction of polarization. This leads to convective-type terms on the right-hand side of both the density and polarization equations. These are true nonequilibrum terms that cannot be obtained from derivatives of a free energy. They arise because, due to the anisotropy of rod diffusion, a motor cluster crosslinking two filaments can yield a net velocity of the pair, even in the absence of net forces, as shown in Appendix A. This term is absent in descriptions of the hydrodynamics of active polymer solutions and gels *close to equilibrium* proposed on phenomenological grounds on the basis of symmetry argument [23,24,40]. It is therefore a *far-from-equilibrium* contribution to active filament dynamics. Kruse *et al.* [23,24] and Voituriez *et al.* [40] have considered the hydrodynamics of an active polymer solution including explicitly the flow of the solvent. In their formulation activity enters via a chemical potential proportional to ATP concentration. In our approach this corresponds to the density $\tilde{m}$ of active motors. The polarization equation considered in Ref. [40] contains a term like our $\sim\beta\partial_j\rho$ in Eq. (5.22) and is obtained there by allowing a coupling between density and splay deformations in the free energy of the system. In equilibrium polar fluids this term is ultimately responsible for the instability of a uniformly polarized phase to splay deformations [41,42].

A nonequilibrium convective-type term of the form contained on the left-hand side of Eq. (5.22) was included in the hydrodynamic equations introduced by Simha and Ramaswamy [19,20] (building on earlier work by Toner and Tu on flocking [16]) to describe the dynamics of self-propelled nematic particles in a solution. In that case the effect of self-propulsion was incorporated by assuming that the particles have a mean drift in the direction of polarization relative to the solvent, yielding an advection term of the type obtained here.

In the polarization equation it is apparent that rotational effects from polar crosslinks (γ_P) increase the bend stiffness, but do not renormalize the splay elastic constant. Nonpolar crosslinks (γ_{NP}) play a role similar to that of excluded volume corrections in suppressing rotational diffusion. This is not surprising as nonpolar crosslinks enhance nematic order in the system. Filament bundling described by α renormalizes both the splay and bend stiffness and promotes spatial inhomogeneities in the polarization.

Linear stability

To examine the stability of the polarized state we choose the $\hat{\mathbf{y}}$ axis along the direction of broken symmetry and expand the hydrodynamic fields about their equilibrium values as

$$\rho(\mathbf{r}) = \rho_0 + \delta\rho(\mathbf{r}), \tag{5.24}$$

$$\hat{\mathbf{p}}(\mathbf{r}) = \hat{\mathbf{y}} + \delta\hat{\mathbf{p}}_\perp(\mathbf{r}), \tag{5.25}$$

where $\delta\hat{\mathbf{p}} = \hat{\mathbf{x}}\delta\hat{p}_x + O((\delta\hat{p}_x)^2)$. Expanding the fluctuations in Fourier components, the linearized equations are given by

$$\partial_t\rho_{\mathbf{k}} = -[D_\alpha^P k^2 - \alpha\tilde{m}\rho_0 k_y^2 - 2iwk_y]\rho_{\mathbf{k}} + [iwk_x + \alpha\tilde{m}\rho_0 k_x k_y]\rho_0\hat{p}_{\mathbf{k}}, \tag{5.26}$$

$$\partial_t \hat{p}_{\mathbf{k}} = -[K_\alpha(\hat{\mathbf{k}})k^2 + iw'k_y]\hat{p}_{\mathbf{k}} + [iw''k_x - D'_\alpha k_x k_y]\frac{\rho_{\mathbf{k}}}{\rho_0}, \tag{5.27}$$

where

$$w = \frac{7}{36}\tilde{m}\beta\rho_0, \tag{5.28}$$

$$w' = \frac{1}{36}\tilde{m}\beta\rho_0, \tag{5.29}$$

$$w'' = \frac{13}{36}\tilde{m}\beta\rho_0, \tag{5.30}$$

$$D^P_\alpha = \frac{3}{4}(D - 2\alpha\tilde{m}\rho_0), \tag{5.31}$$

$$D'_\alpha = \frac{1}{4}\left(D + \frac{\tilde{m}}{24}\gamma_{NP}\rho_0 - 6\alpha\tilde{m}\rho_0\right), \tag{5.32}$$

$$K_\alpha(\hat{\mathbf{k}}) = \frac{1}{4}\left(\frac{5}{2}D + \frac{\tilde{m}}{6}\gamma_P\rho_0 - \tilde{m}\alpha\rho_0\right)\frac{k_y^2}{k^2} + \frac{1}{4}\left(\frac{7}{2}D + \frac{\tilde{m}}{6}\gamma_P\rho_0 - 3\tilde{m}\alpha\rho_0\right)\frac{k_x^2}{k^2}. \tag{5.33}$$

Note that $K_\alpha(\hat{\mathbf{k}})$, with $\hat{\mathbf{k}}=\mathbf{k}/k$, is a generalized stiffness for splay ($k_y=0$) and bend ($k_x=0$) deformations. Denoting by ϕ the angle between the wave vector $\mathbf{k}$ and the direction of broken symmetry, the hydrodynamic modes describing the decay of density and polarization fluctuations are given by

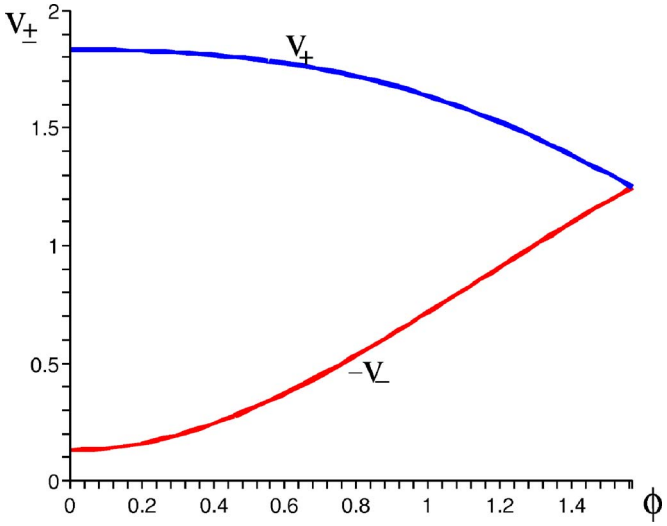

FIG. 6. (Color online) The propagation speeds $v_+(\phi)$ (blue curve online) and $-v_-(\phi)$ (red curve online) of the hydrodynamic modes in the polarized state as a function of the angle ϕ. The speed $v_\pm$ is measured in units of lD_r and we have used $\tilde{m}=1$, $\beta=1$, and $\rho_0=\rho_N$.

$$z_\pm(k,\phi) = ikv_\pm(\phi) - \mathcal{D}^P_\pm(\phi)k^2. \tag{5.34}$$

The modes are always propagating with speed

$$v_\pm(\phi) = (w - w'/2)\cos\phi \pm \sqrt{(w + w'/2)^2\cos^2\phi + ww''\sin^2\phi}. \tag{5.35}$$

The angular dependence of the speed of propagation is shown in Fig. 6. The decay rate is given by

$$\mathcal{D}^P_\pm(\phi) = \frac{1}{2}[D^P_\alpha + K_\alpha(\phi) - \tilde{m}\alpha\rho_0\cos^2\phi] \pm \frac{1}{2}\cos\phi\frac{(w + w'/2)[D^P_\alpha - K_\alpha(\phi) - \tilde{m}\alpha\rho_0\cos^2\phi] + \sin^2\phi(wD'_\alpha - w''\tilde{m}\alpha\rho_0)}{\sqrt{(w + w'/2)^2\cos^2\phi + ww''\sin^2\phi}}. \tag{5.36}$$

For large values of the bundling rate α the various elastic constants are driven to zero and $\mathcal{D}^P_\pm(\phi)<0$, corresponding to the instability of the uniform polarized state. The condition $\mathcal{D}^P_\pm(\phi)=0$ defines the value $\rho_B(\phi)$ of the filament density above which the polarized state is unstable. This value is largest for $\phi=\pi/2$, corresponding to fluctuations with $\mathbf{k}$ normal to the direction of mean polarization (i.e., pure splay deformations of the local polarization) due to the stiffening of the splay elastic constant from polar crosslinks. In contrast, the bend stiffness is not renormalized by polar crosslinks, resulting in a lower value of ρ_B at $\phi=0$, where polarization deformations are pure bend. The angular dependence of $\rho_B(\phi)$ is shown in Fig. 7.

Finally, it is useful to consider explicitly the two limiting cases $\phi=0$ and $\phi=\pi/2$. For $\phi=0$ (i.e., $k_y=k$) density and polarization (in this case bend deformations) fluctuations are decoupled. Their respective relaxation rates are given by

$$z_+(k,\phi) \equiv z_\rho(k,\phi) = 2iwk - \left[\frac{3}{4}D - \frac{5}{2}\tilde{m}\alpha\rho_0\right]k^2, \tag{5.37}$$

$$z_-(k,\phi) \equiv z_p(k,\phi) = -iw'k - \frac{1}{4}\left[\frac{5}{2}D + \frac{\tilde{m}}{6}\gamma_P\rho_0 - \tilde{m}\alpha\rho_0\right]k^2. \tag{5.38}$$

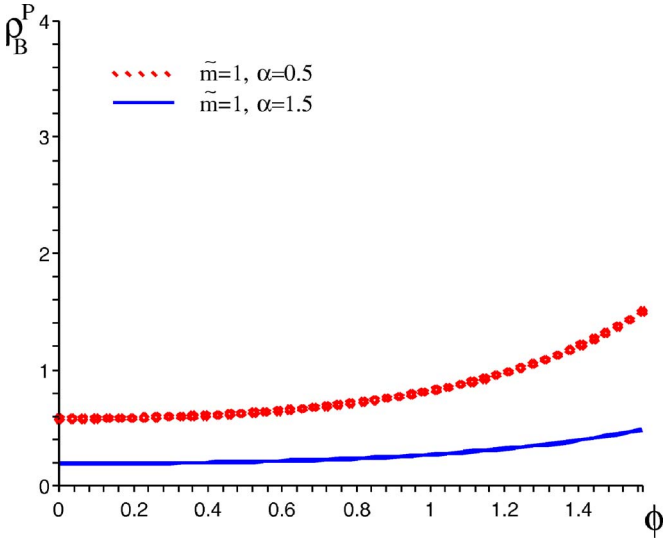

FIG. 7. (Color online) The critical density ρ_B^P where the homogeneous polarized state becomes unstable versus angle ϕ for $D=1$, $\gamma_P=1$, $\gamma_{NP}=1$. As in the nematic phase, by increasing α or $\tilde{m}$ the stable region decreases. The critical density is not very sensitive to changes in γ_P.

The bundling instability is controlled by the growth of density fluctuations and occurs at

$$\rho_B(\phi=0)=\frac{3D}{10\tilde{m}\alpha}. \tag{5.39}$$

For $\phi=\pi/2$ (i.e., $k_x=k$) the modes are complex conjugate, with

$$z_\pm(k,\phi=\pi/2)=\pm ik\sqrt{ww''}-\frac{k^2}{8}(13D/2+\tilde{m}\gamma_P\rho_0/6-9\tilde{m}\alpha\rho_0). \tag{5.40}$$

Both density and splay fluctuations of the polarization field go unstable at the same density, given by

$$\rho_B(\phi=\pi/2)=\frac{13D}{\tilde{m}(18\alpha-\gamma_P/3)}. \tag{5.41}$$

The zipping effect described by γ_P tends to stabilize the system.

D. Summary

All homogeneous states are rendered unstable by the same mechanism of filament bundling, driven by the parameter α. Up to numerical constants and assuming $\gamma_P<\alpha$, the density above which the homogeneous states are unstable can be estimated as $\rho_B\sim D/\tilde{m}\alpha$. The bundling instability line is shown in Fig. 8. One important observation is that the nature of the instability changes from diffusive in both the isotropic and the nematic states to oscillatory in the polarized state. This suggests that at high filament and motor density the uniform polarized state may be replaced by spatially inhomogeneous oscillatory structures such as vortices.

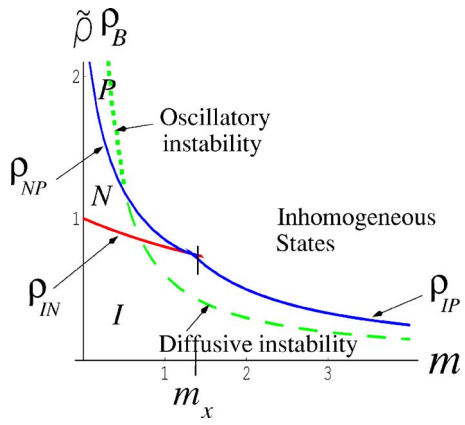

FIG. 8. (Color online) Bundling renders homogeneous states unstable for $\rho_0>\rho_B$, where they are replaced by inhomogeneous solutions. The ρ_B line may lie above the ρ_{NP}-ρ_{IP} line or cross through the N and I states, as shown in the figure ($\gamma_P/\gamma_{NP}=1$, $c_2=50$, $\gamma_{NP}/\alpha=0.6$), depending on the value of γ_{NP}/α. The instability of the I and N states is diffusive (dashed line), while the instability of the P state is oscillatory (dotted line).

VI. DISCUSSION

Several other authors have recently put forward descriptions of the dynamics of active solutions and gels of long biofilaments and molecular motors. It is useful to compare our work to others in some detail.

Kruse *et al.* [23,24] and Voituriez *et al.* [40] have developed a continuum phenomenological description of the polarized state of active polymer solutions where the hydrodynamic equations are written down on the basis of general symmetry considerations. Our work, in contrast, derives such equations from a systematic coarse-graining of a more microscopic kinetic equation. The advantage of the former method is its generality. The disadvantage is that the resulting continuum equations contain many undetermined parameters. Our work yields an estimate for these parameters and an understanding for the microscopic mechanisms that control each term in the continuum equations. On the other hand, the precise dependence of the parameters on the physical properties of the crosslinkers is determined by the specific microscopic model considered, as shown in Appendix A. The two approaches are clearly complementary and both provide insight in the system's dynamics.

The work described in Refs. [23,24,40] explicitly incorporates the dynamics of the solvent, which is assumed quiescent in our work (see, however, Ref. [43]), but consider systems near equilibrium by only keeping terms of first order in the chemical potential, which controls the rate of ATP consumption. For a more precise comparison we refer to Ref. [40], where the equations are written in the simpler form appropriate to an active viscous solution, with no viscoelastic effects. In Ref. [40] activity is controlled by the difference $\Delta\mu$ in the chemical potential of ATP and its hydrolysis products, assumed to be constant. This corresponds in our work to the product $\tilde{m}u_0=\tilde{m}aR_{ATP}$, which controls ATP consumption in the system. All active contributions are proportional to the combinations $\tilde{m}R_{ATP}$. The parameter λ of Ref. [40]

corresponds to our polar rotational rate γ_P, describing the zipping of filaments due to the action of polar crosslinkers and responsible for establishing the homogeneous polarized state. This term is ignored in Ref. [40], where it is assumed from the outset that the system exists in a polarized state with $p_0=1$. The terms proportional to the parameter w arising in the polarization equation of Ref. [40] have the same structure as the first term on the right-hand side of our polarization equation, Eq. (5.22). However, this term is obtained in Ref. [40] as a derivative of a phenomenological free energy, consisting of the usual Frank free energy for a nematic plus a term $\sim w\rho\nabla\cdot\mathbf{p}$, which is allowed in a polar fluid. As a result, this term does not appear explicitly as an active term proportional to $\Delta\mu$. On the other hand, our analysis of the homogeneous states shows that activity is probably crucial for establishing the polarized state as the zipping rate γ_P induced by polar crosslinkers is likely to depend on ATP consumption rate. Furthermore, the convective terms on the left-hand side of Eqs. (5.21) and (5.22) cannot be obtained as derivatives of a free energy and are therefore not present in Ref. [40]. These terms are linear in the ATP consumption rate and are important in controlling the oscillatory nature of the spatial patterns (e.g., vortices) that are obtained at high filament and motor density [35].

Aranson and Tsimring [35] have used a generalization of the Maxwell model of binary collisions in a gas to describe the dynamics of a solution of polar rods with inelastic interaction representing the effect of active crosslinkers. Although their kinetic model, in contrast to ours, allows for instantaneous large changes in the relative angle of two rods upon collision, the continuum equations for density and polarization obtained from the model have the same structure as ours. Our parameter α corresponds essentially to their parameter B^2 (related to the spatial range of the interaction between two rods), while our parameter β is proportional to their parameter H, which controls the strength of the dependence of the interaction between two rods on their relative orientation (although again these authors do not include the convective terms $\sim\beta$ in the density and polarization equations). The dependence on motor density or ATP consumption rate does not appear explicitly in the continuum equations of Ref. [35] as the strength of the motor-mediated interactions is scaled out of the calculation.

One important difference between our work and that of Ref. [35] is that by incorporating excluded volume effects and including the action of both stationary and mobile crosslinkers, we can obtain a complete characterization of the homogeneous states of the system. In particular, we show that both nematic and polar order are possible in different regions of parameters, and evaluate the effect of crosslinks on the isotropic-nematic transition.

Our work can be extended in several ways. First, we have assumed that the solvent is quiescent and only provides the damping on the dynamics of filaments and motors. Relaxing this approximation requires considering explicitly the dynamics of a two-component system. In particular, the dynamics of the solvent must be incorporated when considering the response of the system to an externally imposed flow. This will be discussed in a future publication [43]. Secondly, an analysis of the nonlinear equations for the director and polarization fields in the nematic and polarized phases, respectively, reveals the structure of the possible topological defects in each phase and their stability. This analysis can be carried out partly analytically and partly numerically and can be used to study the range of stability of the spatially inhomogeneous patterns seen in the in vitro experiments by considering each pattern as composed of topological defects of the bulk system. Finally, for comparison with experimental systems it is crucial to consider the dynamics of active solutions in specific geometries, with suitable boundary conditions [44]. An important application of the dynamics of active filament solutions and gels is that of cell locomotion on a substrate. This may be modeled by considering a thin active layer on a substrate, but will require incorporating in the model the nonequilibrium polymerization-depolymerization of the filaments, mechanical coupling to the substrate, and understanding the interplay between them and activity.

ACKNOWLEDGMENTS

We thank Sriram Ramaswamy for useful discussions. This work was supported by the Royal Society (T.B.L.) and by the National Science Foundation, Grant Nos. DMR-0305407 and DMR-0219292 (A.A. and M.C.M.).

APPENDIX A: MICROSCOPIC MODELS OF MOTOR-FILAMENT KINEMATICS

In this appendix we describe some microscopic models of the motor-mediated interaction among two filaments. Clearly such models are a great simplification of the contributions to the motor-mediated forces, but they allow us to estimate the various phenomenological parameters introduced in Sec. II and to justify the approximations used in this paper. We consider two classes of models: (1) small motor clusters with an inhomogeneous stepping velocity that vanishes at the plus end of the filament, inspired by kinesin motor constructs interacting with microtubules; (2) filamentous motor clusters with an antiparallel arrangement of heads inspired by thick myosin filaments interacting with thin actin filaments.

1. Stalling clusters

The model presented here extends the one discussed in Ref. [26] to include the possibility of motor-induced filament rotation. We consider a pair of filaments (denoted as filaments 1 and 2) crosslinked by a motor cluster. Due to the action of the motors, filaments 1 and 2 acquire center-of-mass velocities $\mathbf{v}_1$ and $\mathbf{v}_2$ and rotational velocities $\boldsymbol{\omega}_1$ and $\boldsymbol{\omega}_2$ about the center of mass. Our goal is to evaluate these velocities in terms of the rates at which the motor cluster steps along the filament and rotates relative to it, and of the filaments' orientation. Both filaments and motors move through a solution. We assume that the filament dynamics is overdamped and the friction of motors is very small compared to that of filaments. The coupling of the filaments to the fluid is via a local friction (Rouse model). This is a reasonable approximation for a quiescent solution without externally imposed flow nor flow generated by the motor activity. Under these conditions, hydrodynamic coupling yields logarithmic

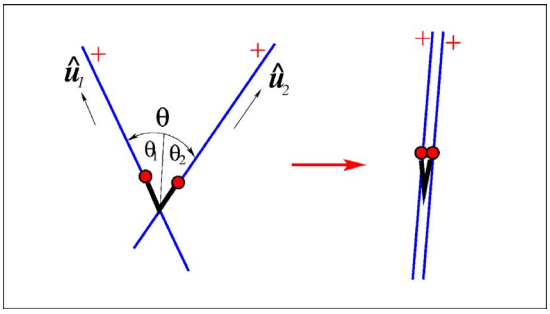

FIG. 9. (Color online) Two filaments of orientation $\hat{\boldsymbol{u}}_1$ and $\hat{\boldsymbol{u}}_2$ connected by an active torsional spring. Here $\theta_i=\theta(s_i)$, for $i=1,2$ is the torsional angle at the point of attachment of the motor cluster. Note that we have chosen a convention such that $\theta=\theta_1-\theta_2$.

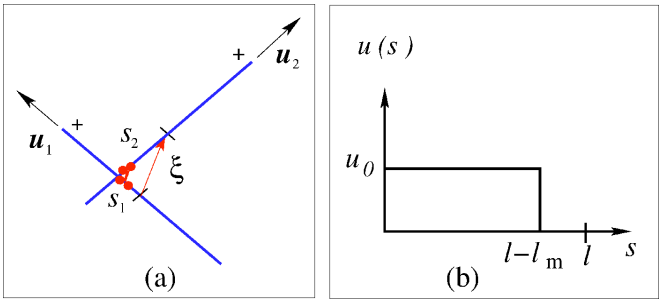

FIG. 10. (Color online) (a) Two filaments connected by an active crosslink and the geometry of the overlap. The filaments' centers are separated by $\boldsymbol{\xi}=s_1\hat{\boldsymbol{u}}_1-s_2\hat{\boldsymbol{u}}_2$. (b) The profile of the motor stepping rate.

corrections to the friction, which are small for long thin rods [9,10,29]. Momentum conservation requires that in the absence of external forces and torques, the total force (torque) acting on filaments centered at a given position be balanced by the frictional force (torque) experienced by the filament while moving through the fluid. The third law requires that any force or torque generated by an active crosslink on one of the filaments of the pair is balanced by an equal and opposite force or torque acting on the other filament. This yields

$$\zeta_{ij}(\hat{\boldsymbol{u}}_1)v_{1j}=-\zeta_{ij}(\hat{\boldsymbol{u}}_2)v_{2j}, \tag{A1}$$

$$\zeta_r\boldsymbol{\omega}_1=-\zeta_r\boldsymbol{\omega}_2, \tag{A2}$$

where $\zeta_{ij}(\hat{\boldsymbol{u}})=\zeta_\parallel\hat{u}_i\hat{u}_j+\zeta_\perp(\delta_{ij}-\hat{u}_i\hat{u}_j)$ is the friction tensor of the rod, with $\zeta_\parallel$ and $\zeta_\perp$ the longitudinal and transverse friction coefficients, respectively, and ζ_r is the rotational friction. Equation (A1) shows that the anisotropy of the friction tensor allows for a net translation $(\mathbf{v}_1+\mathbf{v}_2\neq 0)$ of the filament pair induced by motors.

The mobile crosslink is a small aggregate of molecular motors that exerts forces and torques on the filaments by converting chemical energy from the hydrolysis of ATP into mechanical work. While walking along the filaments, the motor clusters can also apply aligning torques on the filaments, if there is a preferred angle between the heads of the motor cluster. To capture this, we consider the cluster to be a nonlinear torsional spring of size $l_m\sim b\ll l$. A similar description would also be appropriate for any polar crosslinking protein. However, a motor cluster, which aligns the filaments by active contractions, has an ATP-dependent spring constant. A schematic is shown in Fig. 9.

It is convenient to think of the motor cluster as composed of two heads, with the ith head $(i=1,2)$ attached to the ith filament at position $\mathbf{r}_i^\times=\mathbf{r}_i+\hat{\boldsymbol{u}}_i s_i$. Motor heads are assumed to step towards the polar end of filaments at a known speed $u(s)$, which depends on the point of attachment (see Fig. 10). The motor-induced torques occur along the axis of the motor cluster, assumed to be directed perpendicular to the plane containing the filaments, and are capable of generating equal and opposite torques on the two filaments. The torsional angles $\theta(s)$ obey the following equations: $\zeta_r\dot{\theta}(s_1)=-\zeta_r\dot{\theta}(s_2)=-\kappa\sin[\theta(s_1)-\theta(s_2)]\simeq-\kappa[\theta(s_1)-\theta(s_2)]$; κ is the torsional spring constant. In general, the torsional spring constant will also depend on the position of the motor cluster along the filament, i.e., $\kappa=\kappa(s)$. The resulting inhomogeneities in the rotational rate γ does not yield qualitatively new terms in the hydrodynamic equations and will be neglected here (see also Ref. [39]). The dynamics of the ith motor head is described by a translational velocity $\mathbf{v}_i^m$ at the point of attachment and a rotational velocity $\boldsymbol{\omega}_i^m$, given by

$$\mathbf{v}_i^m=\dot{\mathbf{r}}_i^\times=\mathbf{v}_i+u(s_i)\hat{\boldsymbol{u}}_i+s_i\boldsymbol{\omega}_i\times\hat{\boldsymbol{u}}_i, \tag{A3}$$

$$\boldsymbol{\omega}_i^m=\boldsymbol{\omega}_i+(-1)^{i-1}\frac{\kappa}{\zeta_r}\frac{\hat{\boldsymbol{u}}_1\times\hat{\boldsymbol{u}}_2}{|\hat{\boldsymbol{u}}_1\times\hat{\boldsymbol{u}}_2|}, \tag{A4}$$

with $u(s_i)=\dot{s}_i$. Finally, the two motors within a cluster are rigidly attached to each other. This requires

$$\mathbf{v}_1^m=\mathbf{v}_2^m, \tag{A5}$$

$$\boldsymbol{\omega}_1^m=\boldsymbol{\omega}_2^m. \tag{A6}$$

Since the motor cluster has size $l_m\sim b\ll l$, we can neglect the length of the motor compared to that of the filament and assume that the attachment points satisfy $\mathbf{r}_1^\times=\mathbf{r}_2^\times$, or $\boldsymbol{\xi}=\mathbf{r}_2-\mathbf{r}_1=s_1\hat{\boldsymbol{u}}_1-s_2\hat{\boldsymbol{u}}_2$. Equations (A1) and (A2), together with the expressions (A3) and (A4) for the velocities of the motor heads, and the conditions (A5) and (A6) that the two motor heads are rigidly connected, then provide a closed set of equations that can be solved to obtain the filaments' translational and rotational velocities in terms of their relative orientations and of the motors' stepping and torsion rates. It is convenient to introduce relative and net translational and rotational velocities of the filament pair as

$$\mathbf{v}=\mathbf{v}_1-\mathbf{v}_2, \tag{A7}$$

$$\mathbf{V}=\frac{\mathbf{v}_1+\mathbf{v}_2}{2}, \tag{A8}$$

and

$$\boldsymbol{\omega}=\boldsymbol{\omega}_1-\boldsymbol{\omega}_2, \tag{A9}$$

$$\Omega = \frac{\boldsymbol{\omega}_1 + \boldsymbol{\omega}_2}{2}. \tag{A10}$$

For the translational velocities we obtain

$$\begin{aligned}\mathbf{v} &= u(s_2)\hat{\boldsymbol{u}}_2 - u(s_1)\hat{\boldsymbol{u}}_1 + \gamma(s_2 - s_1)(\hat{\boldsymbol{u}}_1 + \hat{\boldsymbol{u}}_2) \\ &\quad + \gamma(1 + \hat{\boldsymbol{u}}_1 \cdot \hat{\boldsymbol{u}}_2)(s_1\hat{\boldsymbol{u}}_1 - s_2\hat{\boldsymbol{u}}_2) \\ &= \frac{1}{2}\{[u(s_2) - u(s_1)] - \gamma(s_1 - s_2)(1 - \hat{\boldsymbol{u}}_1 \cdot \hat{\boldsymbol{u}}_2)\}(\hat{\boldsymbol{u}}_2 + \hat{\boldsymbol{u}}_1) \\ &\quad + \frac{1}{2}\{[u(s_2) + u(s_1)] - \gamma(s_1 + s_2)(1 + \hat{\boldsymbol{u}}_1 \cdot \hat{\boldsymbol{u}}_2)\}(\hat{\boldsymbol{u}}_2 - \hat{\boldsymbol{u}}_1),\end{aligned} \tag{A11}$$

$$\mathbf{V} = A(\hat{\boldsymbol{u}}_2 + \hat{\boldsymbol{u}}_1) + B(\hat{\boldsymbol{u}}_2 - \hat{\boldsymbol{u}}_1), \tag{A12}$$

with

$$\begin{aligned}A = -\frac{\sigma}{4}\left(\frac{1 - \hat{\boldsymbol{u}}_1 \cdot \hat{\boldsymbol{u}}_2}{1 - \sigma\hat{\boldsymbol{u}}_1 \cdot \hat{\boldsymbol{u}}_2}\right) \\ \times[u(s_2) + u(s_1) - \gamma(s_1 + s_2)(1 + \hat{\boldsymbol{u}}_1 \cdot \hat{\boldsymbol{u}}_2)],\end{aligned} \tag{A13}$$

$$B = \frac{\sigma}{4}\left(\frac{1 + \hat{\boldsymbol{u}}_1 \cdot \hat{\boldsymbol{u}}_2}{1 + \sigma\hat{\boldsymbol{u}}_1 \cdot \hat{\boldsymbol{u}}_2}\right)[u(s_2) - u(s_1) + \gamma(s_2 - s_1)(1 - \hat{\boldsymbol{u}}_1 \cdot \hat{\boldsymbol{u}}_2)], \tag{A14}$$

where we have defined $\gamma = \kappa/\zeta_r$ and $\sigma = (\zeta_\perp - \zeta_\parallel)/(\zeta_\perp + \zeta_\parallel)$. For long thin rods $\zeta_\perp = 2\zeta_\parallel \equiv 2\zeta$ and $\sigma = 1/3$.

There is no net rotational velocity of the pair ($\boldsymbol{\Omega} = 0$). The relative rotational velocity is given by

$$\boldsymbol{\omega} = 2\gamma\frac{\hat{\boldsymbol{u}}_1 \times \hat{\boldsymbol{u}}_2}{|\hat{\boldsymbol{u}}_1 \times \hat{\boldsymbol{u}}_2|}. \tag{A15}$$

The fact that $\mathbf{V} \neq 0$ indicates that motor activity can induce a net motion of the pair relative to the solution. This is a consequence of hydrodynamics at low Reynolds numbers, which gives an anisotropic of friction tensor for long thin rods. As a result $\mathbf{V}$ vanishes when $\zeta_\perp = \zeta_\parallel$. Also $\mathbf{V}$ vanishes identically for $\hat{\boldsymbol{u}}_2 = \pm\hat{\boldsymbol{u}}_1$, so that $\mathbf{V} = 0$ in one dimension.

We can compare the expression for the filament velocities obtained via the microscopic model described in this section to the general expression introduced on the basis of symmetry considerations in Eqs. (2.10) and (2.11) by expanding the stepping rate as $u(s) \approx u_0 - su'$, where $u' = -du(s)/ds > 0$. Substituting the expressions $\frac{1}{2}[u(s_1) - u(s_2)] \simeq \frac{u'}{2}(s_1 - s_2)$ and $\frac{1}{2}[u(s_2) + u(s_1)] \simeq u_0 + \frac{u'}{2}(s_2 + s_1)$ into Eq. (A11) we obtain a general expression for the relative velocity given by

$$\mathbf{v} = \alpha_+\hat{\boldsymbol{u}}_+(\boldsymbol{\xi} \cdot \hat{\boldsymbol{u}}_+) + \alpha_-\hat{\boldsymbol{u}}_-(\boldsymbol{\xi} \cdot \hat{\boldsymbol{u}}_-) + \beta(\hat{\boldsymbol{u}}_2 - \hat{\boldsymbol{u}}_1), \tag{A16}$$

where $\hat{\boldsymbol{u}}_+ = (\hat{\boldsymbol{u}}_2 + \hat{\boldsymbol{u}}_1)/|\hat{\boldsymbol{u}}_2 + \hat{\boldsymbol{u}}_1|$ and $\hat{\boldsymbol{u}}_- = (\hat{\boldsymbol{u}}_2 - \hat{\boldsymbol{u}}_1)/|\hat{\boldsymbol{u}}_2 - \hat{\boldsymbol{u}}_1|$ and

$$\alpha_+ = -\gamma(1 - \hat{\boldsymbol{u}}_1 \cdot \hat{\boldsymbol{u}}_2) + u', \tag{A17}$$

$$\alpha_- = \gamma(1 + \hat{\boldsymbol{u}}_1 \cdot \hat{\boldsymbol{u}}_2) + u', \tag{A18}$$

$$\beta = u_0. \tag{A19}$$

If $u' \gg \gamma$, then $\alpha_+ = \alpha_- = \tilde{\alpha}$, leading to the simpler expression for the relative velocity [see Eqs. (2.10) and (2.11)], which we use for the whole of this article.

By comparing Eqs. (A16), (A13), and (A15) to the general expressions given in Sec. II we obtain the following estimates:

$$\tilde{\alpha}_0 \simeq l\left|\frac{du}{ds}\right|, \tag{A20}$$

$$\beta_0 \simeq u_0, \tag{A21}$$

$$\gamma_P \sim \kappa/\zeta_r. \tag{A22}$$

Note that the specific microscopic model used here gives $\tilde{\alpha}_1 = 0$, $\beta_1 = 0$, and $\gamma_{NP} = 0$. This is the result of having considered the kinematics of a single pair of filaments coupled by one motor cluster. An additional dependence of the effective coupling constants is introduced by the dependence of the motor-binding probability on the relative orientation of the filaments.

2. Contractile motor filaments

Here we consider another microscopic model relevant to large contractile filaments of myosin II (thick minifilaments) interacting with filamentous actin (thin filaments). Both the thick contractile motor filament and the thin filaments undergo overdamped motion in a quiescent fluid.

We consider two thin (e.g., actin) polar filaments of length l with centers of mass at $\mathbf{r}_1$ and $\mathbf{r}_2$ and orientations $\hat{\boldsymbol{u}}_1$ and $\hat{\boldsymbol{u}}_2$, respectively. The active crosslink is a (thick) filament of motor proteins of length $l_m < l$. The motor heads within the motor filament are antialigned, with the motor heads at the two ends of the motor filament pointing in opposite directions. Its orientation is described by a unit vector $\hat{\boldsymbol{u}}_m$ oriented along its axis. We choose the direction of $\hat{\boldsymbol{u}}_m$ to be from thin filament 1 to 2, as indicated in Fig. 11. The motor filament exerts torques on the actin filaments by acting as a torsional spring of strength κ. As a result, the actin filaments align with the motor filament, as shown in Fig. 11. Once the thin filaments are parallel to the motor filament, the heads on either side of the motor filament pull the thin filaments together until they overlap over a length $l_m < l$. In this configuration both thin filaments are linked by both heads at the two ends of the contractile motor filament. The effect of these two heads balance and the thin filaments remain stationary relative to each other.

To describe the dynamics, we denote by $\mathbf{v}_m$ and $\boldsymbol{\omega}_m$ the center of mass and angular velocity of the thick motor filament, respectively. The friction tensor of the motor filament is given by $\zeta_{ij}^m = \zeta_{m\parallel}\hat{u}_{mi}\hat{u}_{mj} + \zeta_{m\perp}(\delta_{ij} - \hat{u}_{mi}\hat{u}_{mj})$. Since the thick motor filament is shorter than the two thin filaments it crosslinks, we expect the motor filament translational friction coefficients $\zeta_{m\parallel}$ and $\zeta_{m\perp}$ and rotational friction ζ_{mr} to be smaller than the corresponding parameters for the actin filaments, i.e., $\zeta_{m\parallel} < \zeta_\parallel$, $\zeta_{m\perp} < \zeta_\perp$, and $\zeta_{mr} < \zeta_r$. The separation of

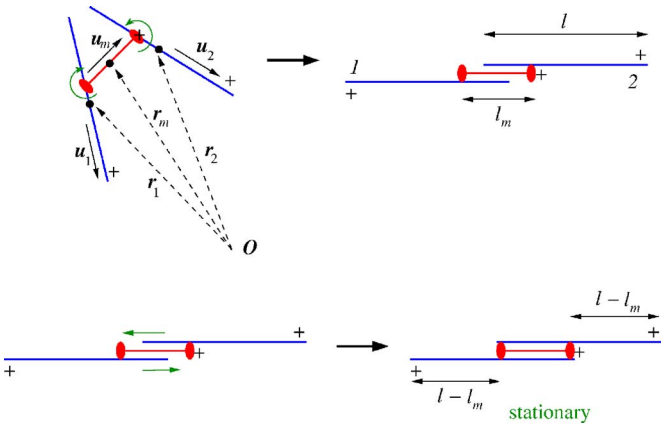

FIG. 11. (Color online) Two thin filaments of length l connected by a contractile thick motor filament of length l_m. Due to the torsional springs, the thick filament aligns the actin filaments in an antiparallel configuration. The "stepping" of motor heads towards the plus ends of the thin filaments bring the (almost) antiparallel filaments together if their centers are more than $l-l_m$ apart. When their centers of mass are separated by $l-l_m$, the two actin filaments are stationary due to the opposing effects of the two motor heads at the opposite ends of the motor filament.

centers of mass of the thin filaments is $\boldsymbol{\xi}\equiv\mathbf{r}_2-\mathbf{r}_1=\hat{\mathbf{u}}_1 s_1 - \hat{\mathbf{u}}_2 s_2+\hat{\mathbf{u}}_m l_m$. Force and torque balance require

$$\zeta_{ij}(\hat{\mathbf{u}}_1)v_{1j}+\zeta_{ij}(\hat{\mathbf{u}}_2)v_{2j}+\zeta^m_{ij}(\hat{\mathbf{u}}_m)v_{mj}=0, \tag{A23}$$

$$\zeta_r\boldsymbol{\omega}_1=\mathbf{G}_1,$$

$$\zeta_r\boldsymbol{\omega}_2=\mathbf{G}_2,$$

$$\zeta_{mr}\boldsymbol{\omega}_m=-\mathbf{G}_1-\mathbf{G}_2, \tag{A24}$$

where

$$\mathbf{G}_1=\kappa(\hat{\mathbf{u}}_m\times\hat{\mathbf{u}}_1),$$

$$\mathbf{G}_2=-\kappa(\hat{\mathbf{u}}_m\times\hat{\mathbf{u}}_2). \tag{A25}$$

The position of the center of mass of the thick motor filament is $\mathbf{r}_m=\mathbf{r}_1+s_1\hat{\mathbf{u}}_1+\hat{\mathbf{u}}_m l_m/2=\mathbf{r}_2+s_2\hat{\mathbf{u}}_2-\hat{\mathbf{u}}_m l_m/2$ and its velocity is given by

$$\mathbf{v}^m_i=\dot{\mathbf{r}}_m=\mathbf{v}_i+u(s_i)\hat{\mathbf{u}}_i+s_i\boldsymbol{\omega}_i\times\hat{\mathbf{u}}_i+(-1)^{i-1}\frac{l_m}{2}\boldsymbol{\omega}_m\times\hat{\mathbf{u}}_m,$$

$$i=1,2. \tag{A26}$$

The set of Eqs. (A26), (A23), and (A24), can be solved for the mean $\mathbf{V}=(\mathbf{v}_1+\mathbf{v}_2)/2$, $\boldsymbol{\Omega}=(\boldsymbol{\omega}_1+\boldsymbol{\omega}_2)/2$ and relative $\mathbf{v}=\mathbf{v}_1-\mathbf{v}_2$, $\boldsymbol{\omega}=\boldsymbol{\omega}_1-\boldsymbol{\omega}_2$ translational and angular velocities of the two thin filaments and the velocity $\mathbf{v}_m$ of the thick motor filament. The general solution is complicated and not terribly transparent.

To simplify the solution, we assume that $l_m\ll l$ so that $\zeta_{mr}\ll\zeta_r$ and $\zeta_m\ll\zeta$. In this case the orientation of the thick motor filament relaxes much faster than that of the two thin filaments and is therefore slaved to the thin filament orientations, so that $\hat{\mathbf{u}}_m=(\hat{\mathbf{u}}_2-\hat{\mathbf{u}}_1)/|\hat{\mathbf{u}}_2-\hat{\mathbf{u}}_1|$. The expressions for the relative and mean velocities are then

$$\mathbf{v}=u(s_2)\hat{\mathbf{u}}_2-u(s_1)\hat{\mathbf{u}}_1+\frac{\gamma}{2}\left\{\frac{(1+\hat{\mathbf{u}}_2\cdot\hat{\mathbf{u}}_1)}{|\hat{\mathbf{u}}_2-\hat{\mathbf{u}}_1|}(\hat{\mathbf{u}}_2-\hat{\mathbf{u}}_1)(s_2+s_1)+\frac{(1-\hat{\mathbf{u}}_1\cdot\hat{\mathbf{u}}_2)}{|\hat{\mathbf{u}}_2-\hat{\mathbf{u}}_1|}(s_1-s_2)(\hat{\mathbf{u}}_2+\hat{\mathbf{u}}_1)\right\}, \tag{A27}$$

$$\mathbf{V}=A(\hat{\mathbf{u}}_2+\hat{\mathbf{u}}_1)+B(\hat{\mathbf{u}}_2-\hat{\mathbf{u}}_1), \tag{A28}$$

where

$$A=-\left(\frac{\sigma}{4}\right)\left(\frac{1-\hat{\mathbf{u}}_1\cdot\hat{\mathbf{u}}_2}{1-\sigma\hat{\mathbf{u}}_1\cdot\hat{\mathbf{u}}_2}\right)\left[u(s_2)+u(s_1)+\gamma\frac{(1+\hat{\mathbf{u}}_2\cdot\hat{\mathbf{u}}_1)}{|\hat{\mathbf{u}}_2-\hat{\mathbf{u}}_1|}(s_2+s_1)\right], \tag{A29}$$

$$B=\left(\frac{\sigma}{4}\right)\left(\frac{1+\hat{\mathbf{u}}_1\cdot\hat{\mathbf{u}}_2}{1+\sigma\hat{\mathbf{u}}_1\cdot\hat{\mathbf{u}}_2}\right)\left[u(s_2)-u(s_1)+\gamma\frac{(1-\hat{\mathbf{u}}_1\cdot\hat{\mathbf{u}}_2)}{|\hat{\mathbf{u}}_2-\hat{\mathbf{u}}_1|}(s_1-s_2)\right]. \tag{A30}$$

The center-of-mass velocity of the thick motor filament is given by

$$\mathbf{v}_m=\mathbf{V}+\mathbf{w}/2, \tag{A31}$$

where

$$\mathbf{w}=u(s_2)\hat{\mathbf{u}}_2+u(s_1)\hat{\mathbf{u}}_1-\frac{\gamma}{2}\left\{\frac{(1+\hat{\mathbf{u}}_2\cdot\hat{\mathbf{u}}_1)}{|\hat{\mathbf{u}}_2-\hat{\mathbf{u}}_1|}(\hat{\mathbf{u}}_2-\hat{\mathbf{u}}_1)(s_1-s_2)+\frac{(1-\hat{\mathbf{u}}_1\cdot\hat{\mathbf{u}}_2)}{|\hat{\mathbf{u}}_2-\hat{\mathbf{u}}_1|}(s_1+s_2)(\hat{\mathbf{u}}_2+\hat{\mathbf{u}}_1)\right\}. \tag{A32}$$

There is no net rotational velocity of the pair ($\boldsymbol{\Omega}=0$) and the relative rotational velocity is given by

$$\boldsymbol{\omega}=2\gamma\frac{\hat{\mathbf{u}}_2\times\hat{\mathbf{u}}_1}{|\hat{\mathbf{u}}_1\times\hat{\mathbf{u}}_2|}, \tag{A33}$$

where $\gamma=\frac{\kappa}{\zeta_r}$.

The speed of the motor clusters depends on the thin filaments' relative position and orientation: it is maximal when the filaments are oppositely oriented and goes to zero when the filament overlaps a length l_m (see Fig. 11). A simple expression that satisfies these conditions is

$$u(s)\simeq\frac{u_0}{2}(1-\hat{\mathbf{u}}_1\cdot\hat{\mathbf{u}}_2)\left[-\left(\frac{1}{2}-\frac{l_m}{l}\right)-s\right], \tag{A34}$$

where u_0 is the (constant) single-motor stepping rate (step size/cycle time).

Assuming $u_0\gg\gamma$ and substituting Eq. (A34) into Eqs. (A27), (A28), and (A33), we obtain an expression for the relative velocity of the two thin filaments connected by a thick filament,

$$\mathbf{v} \simeq u_0(1-\hat{\boldsymbol{u}}_1\cdot\hat{\boldsymbol{u}}_2)\left[\frac{\boldsymbol{\xi}}{l}-\frac{1}{2}\frac{(l-l_m)}{l}(\hat{\boldsymbol{u}}_2-\hat{\boldsymbol{u}}_1)\right], \quad \text{(A35)}$$

where $\boldsymbol{\xi}=s_1\hat{\boldsymbol{u}}_1-s_2\hat{\boldsymbol{u}}_2+l_m\hat{\boldsymbol{u}}_m$. In obtaining Eq. (A35) we used approximated $\hat{\boldsymbol{u}}_m\simeq 1/2(\hat{\boldsymbol{u}}_2-\hat{\boldsymbol{u}}_1)$, which holds when the filaments are antiparallel. By comparing Eqs. (A35) and (A33) to the general expressions given in Sec. II we obtain the following estimates:

$$\tilde{\alpha}_0=-\tilde{\alpha}_1\simeq u_0, \quad \text{(A36)}$$

$$\beta_0=-\beta_1\simeq -\left(1-\frac{l_m}{l}\right)u_0, \quad \text{(A37)}$$

$$\gamma_P=\gamma\simeq\kappa/\zeta_r. \quad \text{(A38)}$$

The crucial difference between the effect of the stalling crosslinker considered in Appendix A 1 and the contractile minifilament considered here is of course that in the present case the rates $\tilde{\alpha}_0$ (β_0) and $\tilde{\alpha}_1$ (β_1) have opposite signs. This will have important effects on the system's rheology.

APPENDIX B: MOMENT EXPANSION

To define the exact moment expansion of the filament concentration $c(\mathbf{r},\hat{\boldsymbol{u}},t)$ we introduce a set of irreducible tensors $T^m_{i_1i_2\cdots i_m}$, which are equivalent to the spherical harmonics, but are expressed in Cartesian coordinates. The components of $T^m_{i_1i_2\cdots i_m}$ are homogeneous polynomials of degree m in the components of the unit vector $\hat{\boldsymbol{u}}$, with the properties that they are fully symmetric in the subscripts $i_1,i_2,\ldots,i_m$, and that no nonvanishing tensor of lower order can be formed by contraction.

Here we denote by d the dimensionality and write the general expression of the T^m for $d=2,3$. Each tensor is orthogonal to all the other ones and normalized according to a product defined by

$$(a,b)=\int\frac{d\hat{\boldsymbol{u}}}{\Omega_d}a(\hat{\boldsymbol{u}})b(\hat{\boldsymbol{u}}), \quad \text{(B1)}$$

where Ω_d is the solid angle in d dimensions, with $\Omega_2=2\pi$ and $\Omega_3=4\pi$. The first few irreducible tensors are

$$T^0=1, \quad \text{(B2)}$$

$$T^1_i=\hat{u}_i, \quad \text{(B3)}$$

$$T^2_{ij}=\hat{u}_i\hat{u}_j-\frac{1}{d}\delta_{ij}, \quad \text{(B4)}$$

$$T^3_{ijk}=\hat{u}_i\hat{u}_j\hat{u}_k-\frac{1}{d+2}[\delta_{ij}\hat{u}_k+\delta_{ik}\hat{u}_j+\delta_{jk}\hat{u}_i], \quad \text{(B5)}$$

$$T^4_{ijkl}=\hat{u}_i\hat{u}_j\hat{u}_k\hat{u}_l-\frac{1}{d(d+2)}[\delta_{ij}\delta_{kl}+\delta_{ik}\delta_{jl}+\delta_{il}\delta_{jk}], \quad \text{(B6)}$$

$$T^5_{ijkls}=\hat{u}_i\hat{u}_j\hat{u}_k\hat{u}_l\hat{u}_s-\frac{1}{(d+2)(d+4)}\times[\hat{u}_i\Delta_{jkls}+\hat{u}_j\Delta_{ikls}+\hat{u}_k\Delta_{ijls}+\hat{u}_l\Delta_{ijks}+\hat{u}_s\Delta_{ijkl}], \quad \text{(B7)}$$

where repeated indices are summed over and the tensor Δ_{ijkl} is given by

$$\Delta_{ijkl}=\delta_{ij}\delta_{kl}+\delta_{ik}\delta_{jl}+\delta_{il}\delta_{jk}, \quad \text{(B8)}$$

it also satisfies $\Delta_{iikk}=d(d+2)$.

The filament concentration has an exact expansion on the basis of these irreducible tensors, given by

$$c(\mathbf{r},\hat{\boldsymbol{u}},t)=\sum_{m=0}^{\infty}a^m_{i_1i_2\cdots i_m}(\mathbf{r},t)\,T^m_{i_1i_2\cdots i_m}(\hat{\boldsymbol{u}}), \quad \text{(B9)}$$

where the mth-order moment $a^m_{i_1i_2\cdots i_m}$ is a tensor determined by

$$a^m_{j_1j_2\cdots j_m}(\mathbf{r},t)\int\frac{d\hat{\boldsymbol{u}}}{\Omega_d}T^m_{j_1j_2\cdots j_m}(\hat{\boldsymbol{u}})T^m_{i_1i_2\cdots i_m}(\hat{\boldsymbol{u}})=\int\frac{d\hat{\boldsymbol{u}}}{\Omega_d}T^m_{i_1i_2\cdots i_m}(\hat{\boldsymbol{u}})c(\mathbf{r},\hat{\boldsymbol{u}},t). \quad \text{(B10)}$$

The first three moments are given by

$$a^0=\int\frac{d\hat{\boldsymbol{u}}}{\Omega_d}c(\mathbf{r},\hat{\boldsymbol{u}},t)=\frac{1}{\Omega_d}\rho(\mathbf{r},t), \quad \text{(B11)}$$

$$a^1_i=d\int\frac{d\hat{\boldsymbol{u}}}{\Omega_d}\hat{u}_i\,c(\mathbf{r},\hat{\boldsymbol{u}},t)=\frac{d}{\Omega_d}\rho(\mathbf{r},t)p_i(\mathbf{r},t), \quad \text{(B12)}$$

$$a^2_{ij}=\frac{d(d+2)}{2}\int\frac{d\hat{\boldsymbol{u}}}{\Omega_d}\left(\hat{u}_i\hat{u}_j-\frac{1}{d}\delta_{ij}\right)c(\mathbf{r},\hat{\boldsymbol{u}},t)=\frac{d(d+2)}{2\Omega_d}\rho(\mathbf{r},t)S_{ij}(\mathbf{r},t). \quad \text{(B13)}$$

Here ρ, $\mathbf{p}$, and S_{ij} are the density, polarization, and nematic order parameter of the rods, respectively. Retaining only moments up to the third one, the filament concentration can be written as

$$c(\mathbf{r},\hat{\boldsymbol{u}},t)\approx\frac{1}{2^{d-1}\pi}\rho(\mathbf{r},t)\left[1+d\hat{\boldsymbol{u}}\cdot\mathbf{p}(\mathbf{r},t)+\frac{d(d+2)}{2}\hat{Q}_{ij}(\hat{\boldsymbol{u}})S_{ij}(\mathbf{r},t)\right], \quad \text{(B14)}$$

with $\hat{Q}_{ij}=\hat{u}_i\hat{u}_j-\frac{1}{d}\delta_{ij}$.

APPENDIX C: DERIVATION OF COARSE-GRAINED CURRENTS

In this appendix we outline the derivation of the currents and source terms entering the equations for the density, polarization, and alignment tensor and give their general form. For simplicity we restrict ourselves to the case of long thin rods, where $D_\parallel=2D_\perp\equiv D$ and $\sigma=1/3$.

It is convenient to separate the translational and rotational currents defined in Eqs. (3.8)–(3.12) in diffusive, excluded volume and active contributions,

$$J_i = J_i^D + J_i^{\rm ex} + J_i^A,$$

$$J_{ij} = J_{ij}^D + J_{ij}^{\rm ex} + J_{ij}^A,$$

$$J_{ijk} = J_{ijk}^D + J_{ijk}^{\rm ex} + J_{ijk}^A, \tag{C1}$$

and

$$R_i = R_i^D + R_i^{\rm ex} + R_i^A, \tag{C2}$$

$$R_{ij} = R_{ij}^D + R_{ij}^{\rm ex} + R_{ij}^A, \tag{C3}$$

where each contribution arises from the corresponding term in Eqs. (2.2) and (2.3).

The diffusive contributions are evaluated by inserting the truncated moment expansion for the filament concentration in the corresponding contributions to the translational and rotational diffusion currents in Eqs. (2.2) and (2.3) and performing the angular average, with the result

$$\mathbf{J}^D = \partial_j \sigma_{ij}^D, \quad \sigma_{ij}^D = -\frac{D}{2}\left(\frac{3}{2}\delta_{ij}\rho + Q_{ij}\right), \tag{C4}$$

$$J_{ij}^D = -\frac{D}{8}(\delta_{ij}\boldsymbol{\nabla}\cdot\mathbf{T} + \partial_i T_j + 5\partial_j T_i), \tag{C5}$$

$$J_{ijk}^D = -\frac{D}{16}(\delta_{jk}\partial_i\rho + \delta_{ik}\partial_j\rho - \delta_{ij}\partial_k\rho) - \frac{D}{6}\left[\delta_{ik}\partial_l Q_{jl} + \delta_{jk}\partial_l Q_{il} + \frac{7}{2}\partial_k Q_{ij} - \delta_{ij}\partial_l Q_{kl}\right], \tag{C6}$$

and

$$R_i^D = D_r T_i, \tag{C7}$$

$$R_{ij}^D = 4D_r Q_{ij}. \tag{C8}$$

To evaluate the excluded volume contributions we expand the concentration in Eq. (2.4) near its value at $\mathbf{r}_1$ as in Eq. (3.2), truncate the moment expansion of the concentration to third order, and perform the angular integrations. Retaining terms up to first order in the gradients of the fields in the currents and up to second order in the source terms, we obtain

$$J_i^{\rm ex} = Dv_0\partial_j\left[-\frac{1}{2}\rho\left(Q_{ij} + \frac{3}{4}\delta_{ij}\rho\right) + \frac{2}{9}Q_{ik}Q_{jk} + \frac{7}{18}\delta_{ij}Q_{kl}Q_{kl}\right] + \frac{2}{3}Dv_0\rho\partial_j Q_{ij}, \tag{C9}$$

$$J_{ij}^{\rm ex} = -\frac{1}{2}Dv_0\left[\frac{1}{4}(\Delta_{ijkl} + 4\delta_{il}\delta_{jk})T_k\partial_l\rho - \frac{1}{9}(\Delta_{ijln} + 6\delta_{in}\delta_{jl})T_k\partial_n Q_{kl} - \frac{1}{9}(\Delta_{ijln} - \delta_{ij}\delta_{ln})T_n\partial_k Q_{kl} - \frac{1}{9}T_k\partial_k Q_{ij}\right], \tag{C10}$$

$$J_{ijk}^{\rm ex} = \frac{1}{12}Dv_0\left\{-\frac{3}{8}(\delta_{ik}\delta_{jl} + \delta_{il}\delta_{jk} - \delta_{ij}\delta_{kl})\partial_l\rho^2 + \frac{1}{3}\rho\partial_l[7\delta_{kl}Q_{ij} + \delta_{ik}Q_{jl} + \delta_{jl}Q_{ik} + \delta_{il}Q_{jk} + \delta_{jk}Q_{il} - 2\delta_{ij}Q_{kl}] - [7\delta_{kl}Q_{ij} + \delta_{ik}Q_{jl} + \delta_{jl}Q_{ik} + \delta_{il}Q_{jk} + \delta_{jk}Q_{il} - 2\delta_{ij}Q_{kl}]\partial_l\rho + \frac{1}{3}\partial_l\left[Q_{ij}Q_{kl} + Q_{ik}Q_{jl} + Q_{il}Q_{jk} - \delta_{ij}Q_{kr}Q_{lr} + (\delta_{il}Q_{jr} + \delta_{jl}Q_{ir} - \delta_{ij}Q_{lr})Q_{kr} + (\delta_{ik}Q_{jr} + \delta_{jk}Q_{ir} - \delta_{ij}Q_{kr})Q_{lr} + \frac{1}{4}(\delta_{ik}\delta_{jl} + \delta_{il}\delta_{jk} - 19\delta_{ij}\delta_{kl})Q_{rs}Q_{rs} + 9\delta_{kl}Q_{ir}Q_{jr}\right]\right\}, \tag{C11}$$

where $v_0 = \frac{2}{\pi}$, and

$$R_i^{\rm ex} = -\frac{1}{3}D_r v_0\left[4T_j Q_{ij} + \frac{1}{6}T_i\nabla^2\rho - \frac{1}{3}T_j\partial_j\partial_i\rho + \frac{1}{18}T_j\nabla^2 Q_{ij} + \frac{1}{9}(T_k\partial_k\partial_j Q_{ij} + T_j\partial_i\partial_k Q_{jk} - T_i\partial_j\partial_k Q_{jk})\right], \tag{C12}$$

$$R_{ij}^{\rm ex} = -\frac{4}{3}D_r v_0\rho Q_{ij} - \frac{1}{288}D_r v_0\left[\rho\left(\partial_i\partial_j\rho - \frac{1}{2}\delta_{ij}\nabla^2\rho\right) + (\delta_{il}Q_{jk} + \delta_{jl}Q_{ik} - \delta_{ij}Q_{kl})\partial_k\partial_l\rho\right]. \tag{C13}$$

To evaluate the active contributions, we insert the gradient expansion of the concentration and motor density given in Eqs. (3.2) and (3.3) in Eq. (2.8) for the motor-current density and in Eqs. (2.5) and (2.6) for the filament currents. The integrals over the lengths s_1 and s_2 of the filaments can then be evaluated explicitly. All terms containing odd powers of components of the filament center of mass separation $\boldsymbol{\xi}$ vanish when averaged over the rods' length. To evaluate the angular integrals in the filament current densities we also expand the translational and rates $\tilde{\alpha}(\theta)$ and $\beta(\theta)$, as well as the excluded volume $|\hat{\mathbf{u}}_1\times\hat{\mathbf{u}}_2| = \sqrt{1-(\hat{\mathbf{u}}_1\cdot\hat{\mathbf{u}}_2)^2}$, to first order in the cosine of the angle between the two filaments, $\hat{\mathbf{u}}_1\cdot\hat{\mathbf{u}}_2$. With this approximation, the motor-induced linear and angular velocities $\mathbf{v}_1 = \mathbf{V} + \mathbf{v}/2$ and $\boldsymbol{\omega}_1$ are written as

$$\mathbf{v} = \frac{\beta_0}{2}(\hat{\mathbf{u}}_2 - \hat{\mathbf{u}}_1) + \frac{\tilde{\alpha}_0}{2}\boldsymbol{\xi} + \left[\frac{\beta_1}{2}(\hat{\mathbf{u}}_2 - \hat{\mathbf{u}}_1) + \frac{\tilde{\alpha}_1}{2}\boldsymbol{\xi}\right](\hat{\mathbf{u}}_1\cdot\hat{\mathbf{u}}_2) + O((\hat{\mathbf{u}}_1\cdot\hat{\mathbf{u}}_2)^2), \tag{C14}$$

$$\mathbf{V} = -\frac{\sigma}{4}\beta_0(\hat{\boldsymbol{u}}_1 + \hat{\boldsymbol{u}}_2) + \frac{\sigma}{4}\tilde{\alpha}_0(\hat{\boldsymbol{u}}_1 s_1 + \hat{\boldsymbol{u}}_2 s_2)$$
$$-\frac{\sigma}{4}[\beta_1 - \beta_0(1-\sigma)](\hat{\boldsymbol{u}}_1\cdot\hat{\boldsymbol{u}}_2)(\hat{\boldsymbol{u}}_1 + \hat{\boldsymbol{u}}_2)$$
$$+\frac{\sigma}{4}[\tilde{\alpha}_1(\hat{\boldsymbol{u}}_1 s_1 + \hat{\boldsymbol{u}}_2 s_2) - \tilde{\alpha}_0(1-\sigma)(\hat{\boldsymbol{u}}_1 s_2 + \hat{\boldsymbol{u}}_2 s_1)](\hat{\boldsymbol{u}}_1\cdot\hat{\boldsymbol{u}}_2)$$
$$+O((\hat{\boldsymbol{u}}_1\cdot\hat{\boldsymbol{u}}_2)^2), \tag{C15}$$

$$\boldsymbol{\omega}_1 = 2[\gamma_P + \gamma_{NP}(\hat{\boldsymbol{u}}_1\cdot\hat{\boldsymbol{u}}_2)]\hat{\boldsymbol{u}}_1\times\hat{\boldsymbol{u}}_2 + O((\hat{\boldsymbol{u}}_1\cdot\hat{\boldsymbol{u}}_2)^2), \tag{C16}$$

and $|\hat{\boldsymbol{u}}_1\times\hat{\boldsymbol{u}}_2|\approx 1$. As indicated in the main text, contributions of higher order in $\hat{\boldsymbol{u}}_1\cdot\hat{\boldsymbol{u}}_2$ only change the values of the numerical coefficients of the various terms in the expressions for the currents given below, but do not contribute any qualitatively new terms.

Finally, we insert the moment expansion of the filament concentration $c(\mathbf{r},\hat{\boldsymbol{u}},t)$, truncate it to the first three moments, as given in Eq. (B14), and evaluate the active contributions to the various current densities defined in Eqs. (3.8)–(3.12). The calculation of the angular integrals is quite lengthy and has been carried out with Maple.

The motor-current density is given by

$$J_i^m = mT_i + \frac{l^3}{48}\left[T_j\partial_i\partial_j m + \frac{1}{2}T_i\nabla^2 m\right] + O(\nabla^3). \tag{C17}$$

The active contribution to the current density is naturally written as the sum of two parts,

$$J_i^A(\mathbf{r},t) = \rho\mathcal{V}_i + \partial_j\sigma_{ij}^A, \tag{C18}$$

where

$$\rho\mathcal{V}_i = -\frac{\tilde{m}}{6}\left(\frac{2\beta_0}{3} + \frac{\beta_1}{2}\right)\rho T_i - \frac{\tilde{m}}{6}\left(\beta_1 - \frac{2\beta_0}{3}\right)Q_{ij}T_j$$
$$+\frac{\tilde{m}\alpha_0}{3}(Q_{ij}\partial_j\rho - \rho\partial_j Q_{ij}) + \frac{1}{3}\left[\alpha_0\rho\left(Q_{ij} + \frac{1}{2}\delta_{ij}\rho\right)\right.$$
$$-\frac{2}{3}\alpha_0\left(Q_{ik} + \frac{1}{2}\delta_{ik}\rho\right)\left(Q_{kj} + \frac{1}{2}\delta_{kj}\rho\right)$$
$$\left.+\frac{\alpha_1}{2}\left(T_iT_j + \frac{1}{2}\delta_{ij}T^2\right)\right]\partial_j m, \tag{C19}$$

and the active contribution to the stress tensor σ_{ij}^A is given by

$$\sigma_{ij}^A = \alpha_0\tilde{m}\rho\left(Q_{ij} + \frac{1}{2}\delta_{ij}\rho\right) + \frac{\alpha_1}{2}\tilde{m}\left(T_iT_j + \frac{1}{2}\delta_{ij}T^2\right), \tag{C20}$$

with $\alpha_0 = \tilde{\alpha}_0/48$ and $\alpha_1 = \tilde{\alpha}_1/48$. The drift $\mathcal{V}_i$ vanishes in a passive system and arises entirely from the contribution to the active current from the net velocity $\mathbf{V}$ of the pair. It is in fact proportional to $\sigma = (\zeta_\perp - \zeta_\parallel)/(\zeta_\perp + \zeta_\parallel)$ and vanishes for isotropic objects. The term proportional to α_0 in the stress tensor describes the buildup of density inhomogeneities via filament bundling and has an effect opposite to that of conventional diffusion. As shown below, this is the main term responsible for driving the instability of homogeneous states.

The active contributions to the translational and rotational polarization currents are given by

$$J_{ij}^A = \tilde{m}\frac{\beta_0}{6}T_iT_j - \frac{\tilde{m}}{6}(\beta_1 - \beta_0/6)\left[T_iT_j + \frac{1}{2}\delta_{ij}T^2\right] - \tilde{m}\frac{\beta_0}{3}\rho\left(Q_{ij} + \frac{1}{2}\delta_{ij}\rho\right) + \frac{\tilde{m}}{6}(\beta_1 + \beta_0/3)\left(Q_{ik} + \frac{1}{2}\delta_{ik}\rho\right)\left(Q_{jk} + \frac{1}{2}\delta_{jk}\rho\right)$$
$$+\frac{\alpha_0}{3}\tilde{m}(T_i\partial_j + T_j\partial_i + \delta_{ij}\mathbf{T}\cdot\boldsymbol{\nabla})\rho + \frac{\alpha_1}{4}\tilde{m}\rho T_{ij} + \frac{\alpha_0}{3}\tilde{m}T_j\partial_i\rho + \frac{2\alpha_0}{3}\tilde{m}T_j\partial_k Q_{ik} + \frac{\alpha_0}{18}\tilde{m}[\delta_{ij}T_l\partial_k Q_{kl} - T_k\partial_k Q_{ij} + T_i\partial_k Q_{kj} - T_k\partial_j Q_{ik}]$$
$$+\frac{\alpha_1}{6}\tilde{m}Q_{jk}T_{ki} + \frac{2\alpha_1}{9}\tilde{m}\left[\frac{1}{2}\delta_{ij}Q_{kl}T_{kl} - Q_{ij}\boldsymbol{\nabla}\cdot\mathbf{T} + Q_{ik}T_{kj} + Q_{jk}T_{ki}\right] + \frac{1}{6}(\alpha_1 + 11\alpha_0/6)\rho(T_i\partial_j + T_j\partial_i + \delta_{ij}\mathbf{T}\cdot\boldsymbol{\nabla})\tilde{m}$$
$$+\frac{2\alpha_1}{9}[Q_{jk}(T_k\partial_i + T_i\partial_k) + \delta_{ij}Q_{kl}T_l\partial_k]\tilde{m} + \frac{1}{9}(2\alpha_1 - \alpha_0/2)[Q_{ik}(T_j\partial_k + T_k\partial_j) + Q_{ij}T_k\partial_k]\tilde{m}, \tag{C21}$$

where

$$T_{ij} = \partial_i T_j + \partial_j T_i + \delta_{ij}\boldsymbol{\nabla}\cdot\mathbf{T}, \tag{C22}$$

and

$$R_i^A = -\gamma_P\tilde{m}\rho T_i + (2\gamma_P - \gamma_{NP})\tilde{m}T_jQ_{ij} - \frac{\gamma_P}{24}\left\{\frac{1}{4}\rho(3\delta_{ij}\nabla^2 - 2\partial_i\partial_j)(\tilde{m}T_j) - \frac{1}{3}\{Q_{ij}(\delta_{jk}\nabla^2 + 2\partial_j\partial_k)(\tilde{m}T_k) + Q_{jk}\partial_j[2\partial_i(\tilde{m}T_k) - 5\partial_k(\tilde{m}T_i)]\}\right.$$
$$\left.+\frac{1}{4}\tilde{m}\rho(\delta_{ij}\nabla^2 + 2\partial_i\partial_j)T_j - \frac{1}{2}\tilde{m}Q_{ij}(\delta_{jk}\nabla^2 + 2\partial_j\partial_k)T_k\right\} - \frac{\gamma_{NP}}{24}\left\{\frac{1}{3}\left[T_j(\delta_{ik}\nabla^2 - \partial_i\partial_k)(\tilde{m}Q_{jk}) + 2T_k\partial_k\partial_j(\tilde{m}Q_{ij}) - \frac{1}{2}T_i\partial_j\partial_k(\tilde{m}Q_{jk})\right]\right.$$
$$\left.+\frac{1}{4}\tilde{m}T_j\left(\partial_j\partial_i - \frac{1}{2}\delta_{ij}\nabla^2\right)\rho + \frac{1}{6}\tilde{m}[T_j(\delta_{ik}\nabla^2 + 2\partial_i\partial_k)Q_{jk} + 2T_k\partial_k\partial_j Q_{ij} - 2T_i\partial_j\partial_k Q_{jk}]\right\}. \tag{C23}$$

Finally, the translational and rotational contributions to the alignment tensor current are

$$J^A_{ijk} = \frac{\tilde{m}}{12}\Bigg\{-\frac{1}{4}\left(\frac{10}{3}\beta_0+\beta_1\right)\rho(\delta_{ik}T_j+\delta_{jk}T_i-\delta_{ij}T_k)+\frac{1}{3}\left(\frac{19}{3}\beta_0-2\beta_1\right)T_kQ_{ij}$$
$$+\frac{1}{6}\left(\frac{5}{3}\beta_0-\beta_1\right)(T_jQ_{ik}+T_iQ_{jk}-\delta_{ij}T_lQ_{kl})+\frac{1}{3}\left(\frac{1}{3}\beta_0-2\beta_1\right)T_l(\delta_{ik}Q_{jl}+\delta_{jk}Q_{il}-\delta_{ij}Q_{kl})\Bigg\}$$
$$+\frac{1}{9}\alpha_0\Bigg\{\tilde{m}\Bigg[\frac{1}{4}(\delta_{ik}\delta_{jn}+\delta_{jk}\delta_{in}-\delta_{ij}\delta_{kn})\rho+\frac{19}{3}\delta_{kn}Q_{ij}+\frac{1}{3}(\delta_{jn}Q_{ik}+\delta_{ik}Q_{nj}+\delta_{in}Q_{jk}+\delta_{jk}Q_{in}-2\delta_{ij}Q_{kn})\Bigg]\partial_l\left(Q_{ln}+\frac{1}{2}\delta_{ln}\rho\right)$$
$$+\frac{11}{2}\Bigg[\frac{1}{4}(\delta_{ik}\delta_{jl}+\delta_{il}\delta_{jk}-\delta_{ij}\delta_{kl})\rho+\frac{1}{3}\delta_{kl}Q_{ij}+\frac{1}{3}(\delta_{jl}Q_{ik}+\delta_{ik}Q_{jl}+\delta_{il}Q_{jk}+\delta_{jk}Q_{il}-2\delta_{ij}Q_{kl})\Bigg]\partial_l(\tilde{m}\rho)$$
$$-\Bigg[\frac{1}{4}(\delta_{in}\delta_{jl}+\delta_{il}\delta_{jn}-\delta_{ij}\delta_{ln})\rho+\frac{1}{3}\delta_{ln}Q_{ij}+\frac{1}{3}(\delta_{il}Q_{jn}+\delta_{jn}Q_{il}+\delta_{jl}Q_{in}+\delta_{in}Q_{jl}-2\delta_{ij}Q_{ln})\Bigg]\partial_l(\tilde{m}Q_{kn})\Bigg\}$$
$$+\frac{1}{6}\alpha_1\Bigg\{\frac{1}{4}\tilde{m}(\delta_{in}T_j+\delta_{jn}T_i-\delta_{ij}T_n)\partial_l(\delta_{kl}T_n+\delta_{kn}T_l+\delta_{ln}T_k)+\frac{1}{3}(\Delta_{vijkln}-3\delta_{ij}\Delta_{klnv})T_v\partial_l(\tilde{m}T_n)\Bigg\}, \tag{C24}$$

where

$$\Delta_{ijkl} = \delta_{ij}\delta_{kl}+\delta_{ik}\delta_{jl}+\delta_{il}\delta_{jk}, \tag{C25}$$

$$\Delta_{ijklnp} = \delta_{ij}\Delta_{klnp}+\delta_{ik}\Delta_{jlnp}+\delta_{il}\Delta_{kjnp}+\delta_{in}\Delta_{kljp}+\delta_{ip}\Delta_{klnj}, \tag{C26}$$

and

$$R^A_{ij} = -2\gamma_P\tilde{m}\left(T_iT_j-\frac{1}{2}\delta_{ij}T^2\right)-\gamma_{NP}\tilde{m}\rho Q_{ij}-\frac{\gamma_P}{48}\Bigg\{\frac{\tilde{m}}{2}(T_i\nabla^2T_j+T_j\nabla^2T_i)+\tilde{m}(T_i\partial_j+T_j\partial_i)\partial_kT_k-\frac{1}{2}\delta_{ij}\tilde{m}(T_k\nabla^2T_k+2T_k\partial_k\partial_lT_l)$$
$$+\frac{2}{3}\Bigg[T_i\nabla^2(\tilde{m}T_j)+T_j\nabla^2(\tilde{m}T_i)-(T_i\partial_j+T_j\partial_i)\partial_k(\tilde{m}T_k)-T_k\partial_i\partial_j(\tilde{m}T_k)-\frac{1}{2}\delta_{ij}[T_k\nabla^2(\tilde{m}T_k)+2T_k\partial_k\partial_l(\tilde{m}T_l)]$$
$$+2T_k\partial_k[\partial_i(\tilde{m}T_j)+\partial_j(\tilde{m}T_i)]\Bigg]\Bigg\}-\frac{\gamma_{NP}}{48}\Bigg\{\frac{\tilde{m}}{2}\rho\Bigg[\partial_i\partial_j\rho-\frac{1}{2}\delta_{ij}\nabla^2\rho+\frac{2}{3}(\nabla^2Q_{ij}+2\partial_i\partial_kQ_{jk}+2\partial_j\partial_kQ_{ik}-2\delta_{ij}\partial_k\partial_lQ_{kl})\Bigg]$$
$$+\frac{\tilde{m}}{3}[Q_{ik}\partial_j\partial_k\rho+Q_{jk}\partial_i\partial_k\rho-Q_{ij}\nabla^2\rho-\delta_{ij}Q_{kl}\partial_k\partial_l\rho]+\frac{2\tilde{m}}{9}[Q_{ik}\nabla^2Q_{jk}+Q_{jk}\nabla^2Q_{ik}+2Q_{il}(\partial_j\partial_kQ_{kl}+\partial_k\partial_lQ_{jk})$$
$$+2Q_{jl}(\partial_i\partial_kQ_{kl}+\partial_k\partial_lQ_{ik})-4Q_{ij}\partial_k\partial_lQ_{kl}-\delta_{ij}Q_{kl}(\nabla^2Q_{kl}+4\partial_l\partial_rQ_{kr})]+\frac{1}{3}\rho[2\nabla^2(\tilde{m}Q_{ij})+\partial_i\partial_k(\tilde{m}Q_{jk})+\partial_j\partial_k(\tilde{m}Q_{ik})$$
$$-\delta_{ij}\partial_k\partial_l(\tilde{m}Q_{kl})]+\frac{1}{3}\Bigg[Q_{ik}\nabla^2(\tilde{m}Q_{jk})+Q_{jk}\nabla^2(\tilde{m}Q_{ik})-2Q_{il}[\partial_j\partial_k(\tilde{m}Q_{kl})-\partial_k\partial_l(\tilde{m}Q_{jk})]-2Q_{jl}[\partial_i\partial_k(\tilde{m}Q_{kl})-\partial_l\partial_k(\tilde{m}Q_{ik})]$$
$$+2Q_{kl}[\partial_i\partial_k(\tilde{m}Q_{jl})+\partial_j\partial_k(\tilde{m}Q_{il})]+3Q_{kl}\partial_k\partial_l(\tilde{m}Q_{ij})-Q_{ij}\partial_k\partial_l(\tilde{m}Q_{kl})-Q_{kl}\partial_i\partial_j(\tilde{m}Q_{kl})-\delta_{ij}Q_{kl}\left(\frac{1}{2}\nabla^2(\tilde{m}Q_{kl})+2\partial_l\partial_r(\tilde{m}Q_{kr})\right)\Bigg]\Bigg\}. \tag{C27}$$

The general nonlinear equations are fairly complicated, but the various terms have simple physical interpretations, as will become apparent below. The terms proportional to α_0 and α_1 tend to bundle filaments together, therefore enhancing density fluctuations. The terms proportional to β_0 and β_1 tend to align the filaments in the direction of the polarization and thus suppress polarization fluctuations. The γ_P and γ_{NP} terms rotate and align filament and play a crucial role in controlling the possible homogeneous states of the system.

APPENDIX D: ROLE OF HIGHER-ORDER GRADIENTS

Here we discuss the role of terms of order higher than second in the gradients of the hydrodynamic fields in controlling the bundling instability. For simplicity we only consider the instability of the isotropic state. In this case the only hydrodynamic variable is the filament density. Including terms of order up to k^4, the dynamics of the Fourier components of density fluctuations defined in Eq. (5.2) is governed by

$$\partial_t \rho_{\mathbf{k}} = -k^2\left[\frac{3}{4}D(1+v_0\rho_0) - \alpha m\rho_0\right]\rho_{\mathbf{k}} + \frac{1}{96}\left[\frac{16}{9}Dv_0\rho_0 - \frac{19}{5}\alpha m\rho_0\right]k^4\rho_{\mathbf{k}}. \quad \text{(D1)}$$

Their decay is controlled by a single diffusive mode, given by

$$z_\rho = -C_2k^2 + C_4k^4, \quad \text{(D2)}$$

where

$$C_2 = m\rho_0(\alpha_c - \alpha), \quad \text{(D3)}$$

$$C_4 = \frac{19}{480}m\rho_0(\alpha_c' - \alpha), \quad \text{(D4)}$$

and

$$\alpha_c = \frac{3Dv_0}{4m}\frac{1+v_0\rho_0}{v_0\rho_0}, \quad \text{(D5)}$$

$$\alpha_c' = \frac{6Dv_0}{6m}. \quad \text{(D6)}$$

At the low-filament densities where the isotropic phase exists, the value α_c where the coefficient C_2 changes sign grows rapidly with filament density, while at the value α_c' where the coefficient C_4 changes sign is independent of ρ_0. We therefore expect $\alpha_c > \alpha_c'$ in the region of interest. We can then identify three regions:

(1) For $\alpha < \alpha_c'$ both C_2 and C_4 are positive. Long-wavelength density fluctuations always decay and the isotropic state is stable. The growth rate defined in Eq. (D2) becomes positive for $k > k_0$, with $k_0 = \sqrt{C_2/C_4}$, but this short-scale instability is outside the range of validity of the present work. We expect that it will be suppressed by terms of even higher order in the gradients.

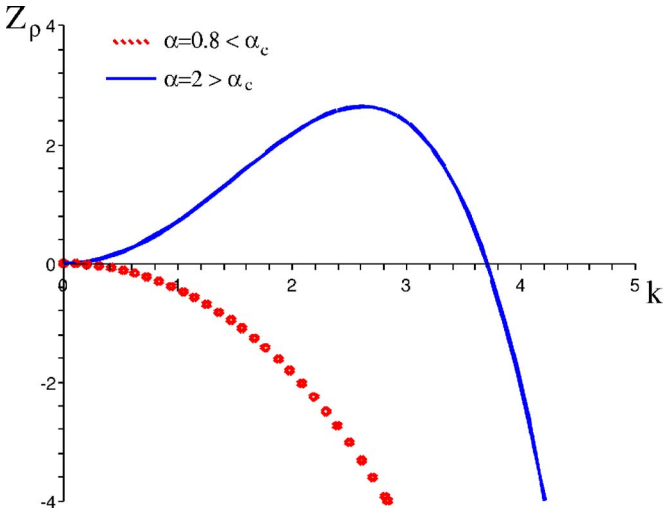

FIG. 12. (Color online) The density mode z_ρ as a function of k for different values of the parameter α for $\tilde{m}=1$, $\rho_0=1$, $\alpha_c' \simeq 0.57$, and $\alpha_c \simeq 1.23$. For $\alpha_c' < \alpha < \alpha_c$ the isotropic state is always stable, and for $\alpha > \alpha_c$ the isotropic state is unstable for long wavelength.

(2) For $\alpha_c' < \alpha < \alpha_c$ we have $C_2 > 0$ and $C_4 < 0$ and the isotropic state is always stable.

(3) For $\alpha > \alpha_c$ the eigenvalue $z_\rho(k)$ controlling the dynamics of density fluctuations becomes positive for $k < k_0$. In this regime long-wavelength density fluctuations grow in time and the isotropic state is unstable. The isotropic state is stabilized again at short scales, $k > k_0 = \sqrt{C_2/C_4}$.

The location of the instability in the (α, ρ_0) is not affected by terms beyond quadratic in the gradients. These terms do, however, introduce a length scale corresponding to the wave vector $k_0 = \sqrt{C_2/C_4} \sim \sqrt{(\alpha-\alpha_c)/(\alpha-\alpha'_c)}$ beyond which the isotropic state is stabilized by short-scale effects as seen in Fig. 12. The wave vector of the fastest-growing mode in the unstable region is $k_m = \sqrt{C_2/2C_4} \sim \sqrt{\alpha_c/(\alpha_c-\alpha'_c)} \sim \epsilon^{1/2}$, that vanishes with the distance $\epsilon = (\alpha-\alpha_c)/\alpha_c$ from the instability.

[1] B. Alberts, A. Johnson, J. Lewis, M. Raff, K. Roberts, and P. Walter, *Molecular Biology of the Cell* (Garland, New York, 2002).
[2] J. Howard, *Mechanics of Motor Proteins and the Cytoskeleton* (Sinauer, New York, 2000).
[3] M. Dogterom, A. C. Maggs, and S. Leibler, Proc. Natl. Acad. Sci. U.S.A. **92**, 6683 (1995).
[4] K. Takiguchi, J. Biochem. (Tokyo) **109**, 520 (1991).
[5] R. Urrutia, M. A. McNiven, J. P. Albanesi, D. B. Murphy, and B. Kachar, Proc. Natl. Acad. Sci. U.S.A. **88**, 6701 (1991).
[6] F. J. Nédélec, T. Surrey, A. C. Maggs, and S. Leibler, Nature (London) **389**, 305 (1997).
[7] T. Surrey, F. J. Nédélec, S. Leibler, and E. Karsenti, Science **292**, 1167 (2001).
[8] D. Humphrey, C. Duggan, D. Saha, D. Smith, and J. Käs, Nature (London) **416**, 413 (2002).
[9] T. B. Liverpool, A. C. Maggs, and A. Ajdari, Phys. Rev. Lett. **86**, 4171 (2001).
[10] T. B. Liverpool, Phys. Rev. E **67**, 031909 (2003).
[11] H. Nakazawa and K. Sekimoto, J. Phys. Soc. Jpn. **65**, 2404 (1996).
[12] K. Sekimoto and H. Nakazawa, in *Current Topics in Physics*, edited by Y. M. Cho, J. B. Homg, and C. N. Yang (World Scientific, Singapore, 1998).
[13] K. Kruse and F. Jülicher, Phys. Rev. Lett. **85**, 1778 (2000).
[14] K. Kruse and F. Jülicher, Phys. Rev. E **67**, 051913 (2003).
[15] K. Kruse, S. Camalet, and F. Jülicher, Phys. Rev. Lett. **87**, 138101 (2001).
[16] J. Toner and Y. Tu, Phys. Rev. E **58**, 4828 (1998).
[17] B. Bassetti, M. C. Lagomarsino, and P. Jona, Eur. Phys. J. B **15**, 483 (2000).
[18] H. Y. Lee and M. Kardar, Phys. Rev. E **64**, 056113 (2001).
[19] R. A. Simha and S. Ramaswamy, Phys. Rev. Lett. **89**, 058101 (2002).

[20] S. Ramaswamy, R. A. Simha, and J. Toner, Europhys. Lett. **62**, 196 (2003).
[21] J. Kim, Y. Park, B. Kahng, and H. Y. Lee, J. Korean Phys. Soc. **42**, 162 (2003).
[22] Y. Hatwalne, S. Ramaswamy, M. Rao, and R. A. Simha, Phys. Rev. Lett. **92**, 118101 (2004).
[23] K. Kruse, J. F. Joanny, F. Jülicher, J. Prost, and K. Sekimoto, Phys. Rev. Lett. **92**, 078101 (2004).
[24] K. Kruse, J. F. Joanny, F. Jülicher, J. Prost, and K. Sekimoto, Eur. Phys. J. E **16**, 5 (2005).
[25] S. Sankararaman, G. I. Menon, and P. B. Sunil Kumar, Phys. Rev. E **70**, 031905 (2004).
[26] T. B. Liverpool and M. C. Marchetti, Phys. Rev. Lett. **90**, 138102 (2003); the full nonlinear equations can be found at http://physics.syr.edu/~mcm/nonlinear_eqs.pdf
[27] A. Ahmadi, T. B. Liverpool, and M. C. Marchetti, Phys. Rev. E **72**, 060901(R) (2005).
[28] J. Uhde, M. Keller, E. Sackmann, A. Parmeggiani, and E. Frey, Phys. Rev. Lett. **93**, 268101 (2004).
[29] M. Doi and S. F. Edwards, *The Theory of Polymer Dynamics* (Oxford University Press, New York, 1986).
[30] T. Shimada, M. Doi, and K. Okano, J. Chem. Phys. **88**, 7181 (1988).
[31] T. B. Liverpool and M. C. Marchetti, Europhys. Lett. **69**, 846 (2005).
[32] D. Smith, D. Humphrey, F. Ziebert, W. Zimmermann, and J. Käs, in *BAPS* (March 2006), U26.00006.
[33] In general the torsional stiffness can also vary along the filament, i.e., $\kappa=\kappa(s)$.
[34] M. Tempel, G. Isenberg, and E. Sackmann, Phys. Rev. E **54**, 1802 (1996).
[35] I. S. Aranson and L. S. Tsimring, Phys. Rev. E **71**, 050901(R) (2005).
[36] P. Kraikivski, R. Lipowsky, and J. Kierfeld, Phys. Rev. Lett. **96**, 258103 (2006).
[37] A. J. Hunt and J. Howard, Proc. Natl. Acad. Sci. U.S.A. **90**, 11653 (1993).
[38] F. Ziebert and W. Zimmermann, Eur. Phys. J. E **18**, 41 (2005).
[39] Spatial inhomogeneities in the torsional spring constant of the crosslinking clusters yield additional terms in Eq. (5.22) proportional to $d\gamma_P(s)/ds$. These terms have the same structure as those proportional to β and therefore do not change the form of the polarization equation. There is, however, an important difference between the contributions proportional to β and those proportional to $d\gamma_P(s)/ds$, in that while the former always arise from motor activity, the latter could also be originated by stationary crosslinks.
[40] R. Voituriez, J. F. Joanny, and J. Prost, Phys. Rev. Lett. **96**, 028102 (2006).
[41] W. Kung, M. C. Marchetti, and K. Saunders, Phys. Rev. E **73**, 031708 (2006).
[42] D. Blankschtein and R. M. Hornreich, Phys. Rev. B **32**, 3214 (1985).
[43] T. B. Liverpool and M. C. Marchetti (unpublished).
[44] M. M. A. E. Claessens, R. Tharmann, K. Kroy, and A. R. Bausch, Nat. Phys. **2**, 186 (2006).